5-2009

Modeling of Compositionally Graded Barium Strontium Titanate From First Principles

Laura Elizabeth Walizer
University of Arkansas

Modeling of Compositionally Graded Barium Strontium Titanate from First Principles

Modeling of Compositionally Graded Barium Strontium Titanate From First Principles

A dissertation submitted in partial fulfillment
of the requirements for the degree of
Doctor of Philosophy in Microelectronics-Photonics

By

Laura Elizabeth Walizer
Hendrix College
Bachelor of Arts in Physics and Philosophy, 2003
University of Arkansas
Master of Science in Physics, 2005

May 2009
University of Arkansas

Abstract

Barium Strontium Titanate ($Ba_xSr_{1-x}TiO_3$ or BST) is a Perovskite alloy of interest for both technological and intellectual reasons. Its ferroelectric and piezoelectric properties make it useful in a variety of electric components such as transducers and actuators, and BST in particular is a material of interest for the development of a ferroelectric RAM for computers. [(1)] The inclusion of $SrTiO_3$, an incipient ferroelectric, and the fact that the properties of a BST system depend strongly on its relative composition of $BaTiO_3$ (BT) and $SrTiO_3$ (ST), make also this a material of high interest. [(2)] Compositionally graded systems are of further interest (see e.g., Refs. (3), (4), (5) and references therein), partly because their compositional grading leads to a built-in polarization gradient. Due to this, these systems could act as transcapacitors, devices which act as charge amplifiers in much the same way that transistors act as current amplifiers. [(3), (4)]

Here, compositionally graded BST systems were modeled using a first-principles derived effective Hamiltonian method within Monte-Carlo simulation. [(6)] The graded systems under consideration had an average Ba composition of 70%. These systems were modeled under stress-free conditions, as well as, under epitaxial strain due to a $SrTiO_3$ substrate.

Both the degree of grading and the thickness of the layers were varied. The investigation revealed that graded BST systems behaved differently from bulk BST systems in several ways. First, some graded BST systems possessed both monodomain states qualitatively similar to those found in bulk systems (except that the polarization exhibited a “wave’’ behavior inside the graded systems), and also states with domain

striping. Where this occurred, the monodomain state was lower in energy, and was therefore the ground-state, but the striped domain state was found to be metastable, representing a local energy minimum.

Analyzing unstrained compositionally graded systems layer by layer revealed that, for small layer thicknesses, the material responded rather homogeneously. However, for large layer thicknesses, each compositionally distinct block responded quite independently, and responded like its equivalent bulk system. This led to some overall systems possessing phases that do not exist in BST bulks (such as monoclinic phases), and to the apparent merging of two phase transitions in unstrained systems.

When compositionally graded BST systems were modeled under a compressive epitaxial strain, only the z-component of the polarization (that is the component along the growth direction) was found to increase from zero below a single critical temperature. As in unstrained systems, some strained systems were found to have monodomain and striped domain states, with the monodomain representing the ground state and the striped domains representing a local minimum.

Development of a BST thin-film code was also undertaken. Initial simulations of BST thin-films were performed using this code, on both disordered and graded systems. These results verified that the new BST thin-film code was functional, as well as revealed interesting phenomena related to compositional grading in two-dimensional materials.

This dissertation is approved for recommendation to the Graduate Council

Major Professor:

_____

Dr. Laurent Bellaiche

Committee Members:

_____

Dr. Greg Salamo

_____

Dr. Reeta Vyas

_____

Dr. Huaxiang Fu

_____

Dr. Hameed Nasseem

_____

Prof. Kenneth Vickers

Dissertation Duplication Release:

Accepted: _____

Laura E. Walizer

Refused: _____

Laura E. Walizer

Acknowledgments

The author would first like to thank her major professor, Dr. Laurent Bellaiche for all of his guidance and support throughout her graduate career, along with postdocs Dr. Sergey Lisenkov and Dr. Inna Ponomareva. She would also like to thank her committee: Dr. Salamo, Dr. Fu, Dr. Vyas and Dr. Nasseem. Special thanks also go to Ken Vickers, and the support staff of the Microelectronics-Photonics department. Last, but by no means least, the author thanks her mother, Elaine, and her father, Donald, for all their encouragement.

The research presented in this work was supported by the Office of Naval Research under grants N00014-04-1-0413, N00014-08-1-0915 and N00014-07-1-0825 (DURIP) and by the National Science Foundation under grants DMR-0701558, DMR-0404335 and DMR-0080054 (C-SPIN). Support was also received from the IGERT program. Any opinions, findings, and conclusions or recommendations expressed in this material are those of the author and do not necessarily reflect the views of the funding agencies.

Table of Contents

Chapter 1: Introduction

The objective of the research presented in this work is to use a first-principles-based, effective Hamiltonian Monte Carlo simulation to model systems based on the Perovskite alloy Barium Strontium Titanate ($Ba_xSr_{1-x}TiO_3$, abbreviated BST). These systems consist of compositionally graded BST superlattices (both stress-free and under epitaxial strain) and some preliminary studies of BST thin-films (both disordered-bulk and compositionally graded). This work follows directly from the research the author presented in her Master's Thesis. [7]

1. Overview and Reasons for Interest

BST is an alloy of two Perovskite compounds, Barium Titanate ($BaTiO_3$, BT) and Strontium Titanate ($SrTiO_3$, ST). Perovskites—a family of crystals whose chemical formulas take the form ABO_3—tend to have a relatively simple crystal structure, which makes them good candidates for theoretical analysis. [8] This crystal structure is illustrated in Figure 1 [9]:

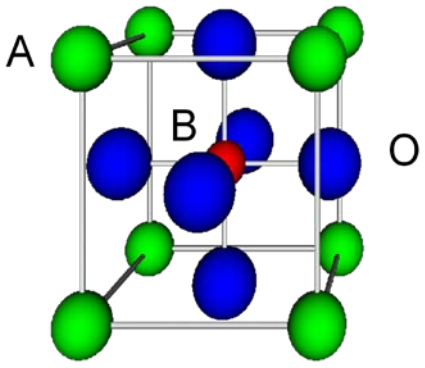

Figure 1: The five-atom unit cell of a perovskite crystal. Ba or Sr occupy the "A" sites, and Ti occupies the "B" sites in BST. (9)

Perovskite compounds also tend to display useful ferroelectric, dielectric and piezoelectric properties, which will be described briefly below. These properties make Perovskites useful in a variety of electric components such as transducers and actuators, which are used in many devices ranging from telephone speakers to sonar. [10]

While Barium Titanate is a very ordinary Perovskite—indeed, it has been referred to as "the canonical ferroelectric crystal" [11]— some of the purely intellectual interest in BST systems arises from the involvement of Strontium Titante in the mix. This is because ST, by itself, is an incipient ferroelectric. This means that classical theory predicts that ST should be a typical Perovskite and display ferroelectric behavior at low temperatures. However, the expected ferroelectric behavior never appears in experiments, all the way down to 0K, due to (1) the presence of a competing antiferrodistortive phase (where the energy of the system is minimized by rotating the oxygen octahetra, rather than by undergoing a ferroelectric transition) and (2) non-classical low-temperature effects, in particular zero-point phonon motions. [11]

Ferroelectric behavior can, however, be induced in ST by the introduction of impurities, such as BT, above a critical concentration. For BST, this concentration is just below a composition of x=0.1. The exact mechanism by which ferroelectric behavior is induced has been disputed, [2], [12] and this is one more reason for the intellectual interest in BST systems. Also, the properties of a BST alloy depend strongly on its relative composition of BT and ST. [2] This is why BST is of interest for its dielectric properties, which make it useful in capacitors, the precise behavior of which could be "tuned" by choosing the proper composition. [2] The ferroelectric behavior of BST also makes it a

material of interest for developing a new form of random access memory (RAM) for computers. [1]

While the above applies equally to all BST systems, there are reasons to be particularly interested in compositionally graded BST systems. First, graded BST systems can display phases not found in bulk BST. Second, graded ferroelectric systems can act as "transcapacitors," [3], [13], [14] which might allow these materials to be used for pyroelectric applications. [13], [3] The nature of this property and its origins will be discussed in greater detail below.

2. Basic Background Information

It is first important to establish exactly what a graded BST system is for purposes of this work, and to define the terms used to describe these systems. In contrast to a disordered bulk BST system, in which the whole of the simulated material consists of a single relative composition of Ba and Sr, a graded BST system is a system which consists of alternating blocks of differing compositions. Such graded systems can be distinguished by the number of different compositions involved, and by the thickness (denoted by the variable n) of each block of unique composition. For example, a graded system could have blocks of 40% Ba BST alternating with pure BT, with the blocks each being three five-atom perovskite cells thick. Such a system would be said to be a two-tiered system with n=3. Another system might have blocks of 40%, 70% and 100% Ba, respectively, with each block being two perovskite cells thick. This would be a three-tiered system with n=2. For added clarity, these cases are illustrated below in Figure 2:

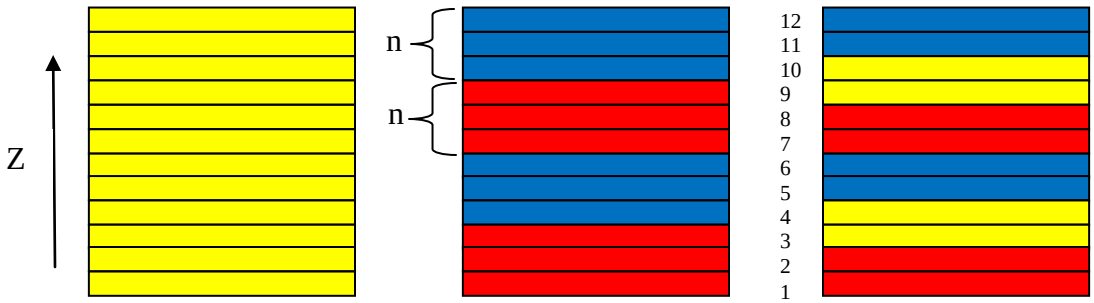

Figure 2: Illustrating graded BST systems. A bulk BST supercell 12 perovskite cells (or layers) thick is shown at left. A supercell with two-tiered grading and an n of 3 is shown at center, and a system with three-tiered grading and n=2 is shown at right. Different compositions are shown in different colors. Brackets illustrate region thickness (n) measured in the number of perovskite cells (or layers) in the z-direction. The layer index is shown on the right-hand figure.

These graded systems, like disordered bulk systems, display ferroelectric, dielectric and piezoelectric behaviors. The ferroelectric effect occurs in crystals whose structures allow them to gain stability by forming permanent dipole moments at each crystal site.[15] These dipole moments will have two or more possible orientations, and in a newly formed crystal the dipole moments will be distributed randomly among the possible orientations.[15] At best, there will be small pockets of dipoles aligned the same way, called domains, and the crystal will have no overall macroscopic polarization.[16] However, when the crystal is exposed to an electric field, all the individual dipoles will orient to the field and therefore will be aligned in the same direction, and the whole crystal will then possess a permanent dipole moment which will not disappear in the absence of the applied field. This will be true so long as the temperature of the crystal is not so high that the dipoles have the necessary energy to spontaneously change orientation.[15] Therefore, each ferroelectric crystal has a temperature above which no ferroelectric behavior occurs, but below which it does occur, and this temperature is called the Curie temperature, T_c.[16]

When a ferroelectric crystal is exposed to a changing electric field and the polarization response is measured, this response takes the form of a hysteresis loop, exactly analogous to the hysteresis loop created by a ferromagnet exposed to a changing magnetic field. A typical example is shown in Figure 3 [17]:

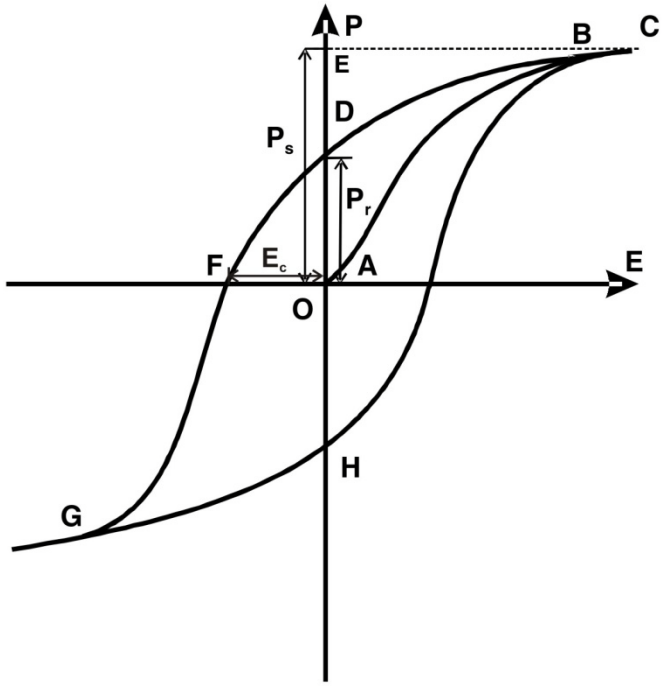

Figure 3: A typical hysteresis loop. (17)

When a new crystal is first exposed to a field, the response follows the curve from point O to point B. When the applied field becomes sufficiently large, the polarization will reach a maximum, or saturation, value, $\mathbf{P_s}$. If the applied field is then decreased smoothly to zero, it will be found that the crystal still carries some polarization, which is referred to as the remnant polarization, $\mathbf{P_r}$. The electric field may also be applied in the opposite direction, relative to its original orientation. Such a field, when strong enough,

would ultimately reverse the direction of the polarization, and this case completes the hysteresis loop. [17]

At temperatures above T_c, a ferroelectric crystal is said to be in a paraelectric state, and it shows a dielectric response but not a ferroelectric response. [16] In this case, the material becomes polarized when exposed to an applied electric field, but the polarization vanishes when the field is removed. It may be most simply understood by imagining the material has a center of positive charge and a center of negative charge. Normally, these coincide, but when a field is applied, they become displaced from one-another. The magnitude of the charge displaced and the distance of the displacement are measured as the "dipole moment". This concept is illustrated in Figure 4 [18]:

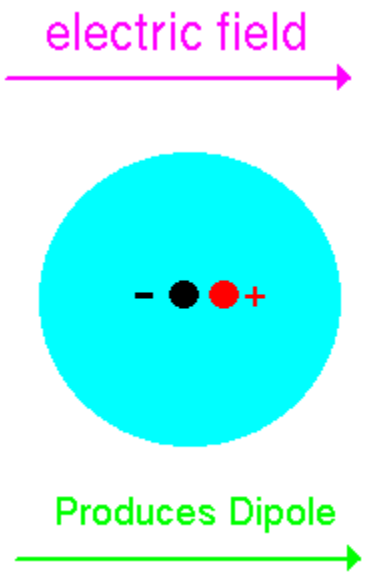

Figure 4: illustrating the dielectric effect.

The applied field **E** and the resulting induced polarization $\mathbf{P}^{ind}$ are directly proportional, and the constants of proportionality form the susceptibility tensor, χ_{ij}. The relationship is given by Equation 1, where i and j represent Cartesian coordinates:

$$P_i^{ind} = \chi_{ij} E_j$$

Equation 1

Other prominent effects occurring in ferroelectric crystals are the pyroelectric and piezoelectric effects. The pyroelectric effect is a phenomenon in which a crystal initially at high temperature shows no polarization even under a very strong applied field, but when the temperature of the crystal is changed, a polarization spontaneously appears. All ferroelectric materials are also pyroelectric, though the reverse is not necessarily true. [16] That is because ferroelectricity requires the polarization to be reversible, while this is not a requirement for pyroelectricity.

All ferroelectric crystals are also piezoelectric, though not necessarily the reverse. [16] A piezoelectric material produces a polarization when under applied stress (the piezoelectric effect) and the material will experience a strain when exposed to an electric field (the reverse piezoelectric effect). The latter is illustrated in Figure 5 [19], while the governing equations of this effect are given in Equation 2 and Equation 3 [20]:

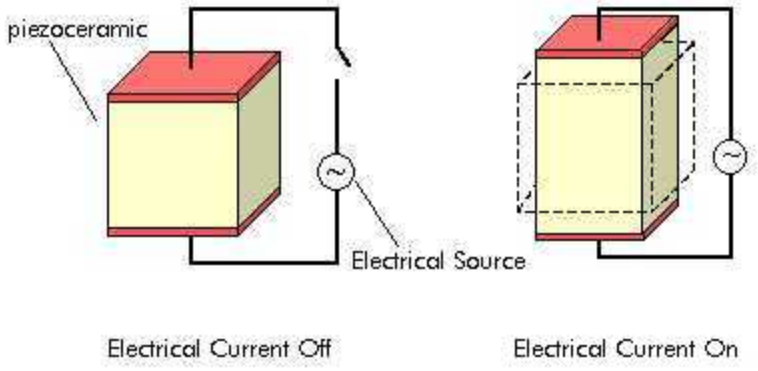

Figure 5: The piezoelectric effect

$$P_i^{ind} = d_{ij}\sigma_j$$

Equation 2

$$\eta_j = d_{ij}E_i$$

Equation 3

$\mathbf{P}^{\mathbf{ind}}$ is the induced polarization due to a stress, $\boldsymbol{\sigma}$, $\mathbf{E}$ is the applied electric field and η is the resulting strain, and the elements d_{ij} are referred to as the piezoelectric coefficients.

All of these effects occur in both bulk and graded ferroelectrics. However, graded ferroelectrics, such as the compositionally graded BST systems under consideration, display one more important behavior. The hysteresis loop produced by a graded material is no longer centered on the origin—like the loop shown in Figure 3—but is instead displaced along the polarization (or charge) axis. [13], [21], [22] This displacement can be

either up or down, and the direction depends on the direction of the compositional gradient relative to the substrate the material sits on. This displacement of the hysteresis loop is shown in Figure 6 [21].

This occurs because the compositional gradient causes the material to have a "built in" polarization gradient. [21], [22] An identical polarization gradient—with the accompanying offset of the hysteresis loop—can be induced by subjecting a bulk material to a temperature or strain gradient. [14], [21] This is cited as proof that the polarization gradient is indeed intrinsic to the graded material, and that it is not an artifact of the electrodes involved or other contact effects. [3], [14], [22]

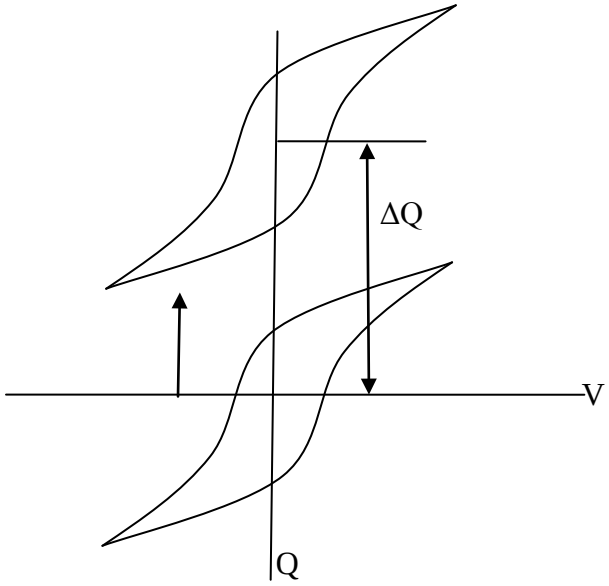

Figure 6: An offset hysteresis loop, redrawn from reference (21).

One consequence of the hysteresis offset which has generated a great deal of interest is the potential for these materials to act as "transcapacitors". [3], [14], [22] Because

of the built-in polarization gradient, these materials have an asymmetric charge-voltage characteristic, the same way transistors have an asymmetric current-voltage characteristic. [3], [22] Therefore, these compositionally graded materials act as charge amplifiers in the same way that transistors act as current amplifiers, [14] and hence the use of the term "transcapacitors". While the potential technological applications of this behavior are likely to be many, the author is not yet aware of any specific uses being proposed.

3. Current Related Research

Some recent studies which are pertinent to the current work are studies of Lead Zirconate Titanate, P(Zr,Ti)O3 or PZT, thin-films, performed here at the University of Arkansas. One study (23) examined PZT films under stress-free, open-circuit boundary conditions. It used a method very similar to that described later in Chapter 2 (section 3) but used an Effective Hamiltonian whose form and coefficients were appropriate to PZT rather than BST. This study examined films one to six primitive cells thick under open-circuit boundary conditions and found that the short-range interactions were highly influenced by surface termination effects, and this led to a decrease in Curie temperature in the 50% Ti PZT film relative to the corresponding bulk PZT system. Further, a monoclinic phase, in which polarization was non-zero along two Cartesian axes but which polarizations were not of equal magnitude, was observed for some relative compositions of Ti, a phase which was not observed in bulk PZT. (23)

A subsequent paper [24] by Kornev, Fu and Bellaiche examined the effects of compressive and tensile strains on 50% Ti PZT systems of five unit cell thickness with varying but incomplete compensation of the depolarization field. Under stress-free conditions, the system was found to be in a tetragonal phase in which the polarization was nonzero along the z-axis at the smallest value of depolarizing field considered. As the depolarizing field increased, the system entered a monoclinic M_A phase in which there was polarization along all three axes but that in the z-direction was greater than that in the x-and y directions, the latter two components being equal to one-another. Next it entered a "triclinic" phase where all components of the polarization were greater than zero, but not none were equal to one-another. Next, it entered another monoclinic phase designated M_C, in which the x-component of polarization was zero, and the y- and z-components were nonzero but nonequal. Finally, the material showed a tetragonal phase for the highest values of depolarizing field, in which only the y-component of polarization was greater than zero. [24] The system under tensile strain exhibited an M_A phase at the least depolarizing field, through a triclinic phase, to an M_C phase at the highest value of depolarizing field. [24] Finally, the system under compressive strain showed a tetragonal phase for lower depolarizing fields, and a macroscopically nonpolar phase at greater values of the depolarizing field, because the compressive strain suppressed in-plane coordinates of the polarization. [24] This represented a level of detailed understanding which could not be previously achieved in either experiment or simulation. [24]

Even more recently, Bin-Omran, Ponomareva, and Bellaiche [25] studied PZT films of 50% Ti composition under near short-circuit boundary conditions at low

temperature (10K), and compared the behavior of these systems to the behavior of BT films of varying thicknesses, and under varying mechanical boundary conditions (i.e., strains). It was first noted that the z-component of the polarization increased at a given compressive strain with decreasing film thickness, due to enhancement of the polarization near the film surface. [25] Also, for perfect SC conditions it was found that the polarization decreased in PZT bulk with increasing compressive strain. This was opposite to the behavior of BT bulk and the thinnest PZT film studied, though the slope of the polarization-versus-strain was much smaller in the PZT film than in the BT bulk. This showed that there was no universality in the strain-dipole coupling in Perovskite systems, unlike what was previously thought. [25] The polarization-versus-strain slope for the thinnest film examined became negative again when the magnitude of the depolarization field was increased. [25]

More generally, a study by Ponomareva et al. [26] presented a dipole-dipole interaction model which allowed one to compute the depolarizing field in a self-consistent manner in 3, 2, and 1 or even 0 periodic dimension(s). The model was tested on a PZT quantum dot of 60% Ti composition. [26] Under OC boundary conditions, a toroidal moment, in which the individual dipoles are arranged in a vortex pattern, was found. Due to this vortex arrangement of the dipoles, the macroscopic dipole moment was zero but the system still possessed a nonzero order parameter, which was the so-called toroidal moment. [27] Under near-ideal SC conditions, the dot was found to exhibit a non-zero macroscopic polarization, and no toroidal moment. [26]

A closely related study examined so-called nanodisks and nanorods—i.e., dot-like cylindrical nanostructures whose diameter was either greater (disks) or less than (rods)

the height of the cylindar—in a paper published in Nature. [27] This study examined nanoparticles composed of 50% Ti PZT which were freestanding (i.e., surrounded by vacuum), and results were presented for systems with a cylindrical height of 14 times the bulk lattice constant. It was found that phase transitions did indeed occur in these systems but, like the case of the dot examined by Ponomareva et al., [26] these transitions involved a toroid moment rather than a dipole moment. The results showed that below a critical diameter (six times the bulk lattice constant) no macroscopic toroid or dipole moment was found, a phase denoted SG for spin-glass. [27] Systems with diameters between six and eight times the bulk lattice constant displayed four vortices appearing in the central x- and y-cross-sections, arranged vertically. These vortices were found to have a diameter approximately equal to the diameter of the nanorod, and each neighboring vortex had an opposite toroid moment. Also, the edges of the vortices in one plane crossed the center of the vortices in the other, leading to an overall helical arrangement of dipoles. [27] Systems with diameters of greater than eight times the bulk lattice constant were found to have a vortex in each x-y plane going either clockwise or counterclockwise about the z-axis. The toroid moment of this phase increased with increasing diameter, the moment-versus-diameter curve having an inflection point where the diameter and height were equal. For nanorods, the Curie temperature increased as the diameter increased, but the Curie temperature of nanodisks was not found to vary with the diameter. [27] These toroid-based phases may prove useful in the development of ferroelectric data-storage, as the direction of the cortices can be switched and the lack of a dipole moment largely avoids the problem of ‘cross-talk’ between adjacent memory units. [27]

Moving away from low-dimensional systems and on to suplerlattices, one also finds much illuminating research taking place. Perhaps the first step in understanding graded materials—and a convenient segue from the topic of films—is a theoretical understanding of how strain influences the behavior of films. In order to study the internal stresses in PZT films of 80% Ti composition, Roytburd et al. [28] derived a relation between the polarization response of a given film and its elastic response, utilizing the Gibbs free energy. The derived relation was then applied to the PZT films, and the theoretical value of the internal stress (1.15 GPa) was found to be in very good agreement with the value calculated based on the experimentally found polarization (1 GPa). The authors did not expect every experiment of this type to yield such close results, but they did expect that their method could be used to obtain at least reasonable estimations of internal stress. [28]

This is valuable knowledge when seeking to understand superlattices, since superlattices can in some cases be understood as several thin-films of differing compositions stacked on top of one-another. Such an understanding was exploited by Roytburd and Slutsker [29] when using thermodynamic principles to model the evolution of polarization in superlattices and graded films. The superlattice was found to have a monodomain with homogeneous polarization and a domain within which were 180-degree, vertically striped domains. As the applied field increased, the fraction of the material occupied by the monodomain grew wider in the z-direction, and the “up” striped domains (i.e., those with a polarization parallel to the applied field) grew wider in-plane (i.e. in the x direction) at the expense of the “down” striped domains (i.e., those having polarization antiparallel to the applied field). A graded material was found to have a

similar starting configuration, but the striped domains expanded into wedge shapes which then grew into single domain states in each layer in succession. [29]

Sepilarsky et al. [30] studied the long-range ferroelectric interactions in $KNbO_3/KTaO_3$ (KNO/KTO) superlattices. These authors used shell-model potentials to run atomic-level simulations of the KNO/KTO superlattices. They found that, for these systems, the in-plane polarization components were generally weakly coupled across the interfaces of KNO and KTO regions, while the growth-direction (z) components were strongly coupled across interfaces. When the total thickness of a KNO/KTO layer was less than 12 unit-cells thick, interaction between layers was strong enough such that the material behaved as a single unit, but for greater thicknesses the behavior of KNO and KTO regions became increasingly decoupled. [30]

Ban, Alpay and Mantese [21] more generally examined the basic theoretical properties of graded ferroic materials using Landau-Ginsburg theory to derive the free-energy of such systems, and from there derived the charge offset of BT/ST superlattices, thus verifying the origin of the displacement of the hysteresis loops of such systems. [21] This theoretical understanding was then applied to other aspects of superlattices in subsequent research.

Zhong, Alpay and Mantese [31] used the free energy to theoretically calculate the tunability—that is, the change in dielectric response under an applied electric field as compared to the response with no applied field—of BT/ST superlattices with varying relative fractions of ST. They found that both a stress-free system and an equivalent system modeled under strain as from an ST substrate showed very high (≈ 97%) tunability when their respective compositions of ST were 15% and 70%. Their dielectric

responses also showed sharp peaks at these relative compositions. This nearly ideal performance, which is superior to that of non-graded thin-films, is thought to hold great promise for practical applications. [31]

Applying a strain to a graded ferroic material was also found by Akcay et al. [32] to affect the magnitude of the charge offset of the hysteresis loop in graded BST thin-films whose components ranged in composition from 70%-100% Ba. Under tensile strain, and "moderate" compressive strain, the polarization of the more Barium-rich layers was greater than that of the less Barium-rich layers, as would generally be expected. [32] However, at compressive strains of greater than approximately 9%, this polarization profile—and therefore the charge offset—became reversed. Thus, by using different substrates or by varying the applied strain through other methods, one can control the degree and even direction of charge offset, a property which is of great interest for such applications as infrared detectors and tunable microwave devices. [32]

Using a nonlinear thermodynamic model that incorporated electrical, mechanical and electromechanical interactions between the layers of a graded BST system, Zhong, Aplay and their colleagues [33] were able to analyze a graded system comprised of layers of 60%, 75% and 90% BT. They were able to theoretically and experimentally demonstrate that the heterostructure in question had high tunability over a relatively wide range of temperatures (compared to non-graded thin-films) because the blocks of differing composition each had different Curie temperatures, making the transition of the material as a whole more "diffuse" and thus broadening the peak dielectric response. [33]

Other studies found that the piezoelectric properties of graded materials were also enhanced. Nath et al. [34] found that a graded BST thin-film with the same grading

scheme as that used in the previous study [33] displayed as much as a 50% improvement in piezoelectric response compared to a 60% BST thin-film. These films were grown by metal-organic solution deposition, and their responses measured by piezoresponse force microscopy. [34] The responses of both films were similar for applied voltages of 2V or less, and for applied voltages greater than 7.5V. In the low-voltage cases, this is explained by the fact that neither film has completely polarized, while the similarity of the high-voltage cases was explained by the dominance of dielectric, rather than piezoelectric, responses at these voltages. [34] In the range between 2 and 7.5V, however, the graded film did indeed show significantly greater piezoelectric response, the greatest enhancement occurring around 4.5-5V. This enhancement was attributed to the built-in strain and polarization gradient occurring in the compositionally graded film. [34] Another study by Zhong et al. [35] examined graded BST and PZT films and found that both materials exhibited superior displacement-versus-field behavior and large piezoelectric strains. [35] This agreed well with Nath's findings.

Competing with (or complementing) the effective Hamiltonian model which will be described below, there exists a so-called shell-model. This technique treats atoms in a crystal as a massive core (the nucleus and inner-orbital electrons) surrounded by a masses shell (the valence electrons). [36] A potential energy based on the electrostatic interactions of these shells is then derived and used as the centerpiece of a molecular dynamics simulation. These simulations are capable of modeling the dynamic properties of a material, while the effective Hamiltonian approach uses thermodynamic principles to model the thermal behavior of the subject material. [36] Earlier and simpler versions of the shell technique use only lower-order terms for the interaction energy, and treat the

polarizability of atoms as isotropic. [37] In order to model perovskites such as bulk $BaTiO_3$, it is necessary to include anharmonic and anisotropic effects. [36], [38] Tinte et al. used this approach to model bulk BT [36] and disordered-bulk BST. [39]

In studying BT, Tinte et al used an anisotropic shell model, and were able to reproduce an energy function with two minima, as required for ferroelectric behavior, and the variance of the total energy versus the crystal lattice parameter. They were also able to qualitatively reproduce the transition pattern of BT, though the transition temperatures found were far below experimentally obtained values. [36] Because the previous work underestimated the transition temperatures of BT, the first step in modeling BST in ref (39) was to modify the shell model for BT to correct the discrepancy. This was practically done by doubling the depth of the troughs in the total energy function. This yielded transition temperatures for BT in much closer agreement with experiment. The shell model was then parameterized for ST. Randomly disordered supercells were then prepared, and the correct parameters (BT or ST) were applied for a given unit cell. A phase diagram of transition temperatures for varying relative compositions was ultimately produced using this method.

It is noted that quantum effects were not included in either the work of Tinte or the work presented in the author's master's thesis. The phase diagrams resulting from the competing shell-model and effective Hamiltonian methods were compared briefly in the thesis, and the effective Hamiltonian approach was asserted to be superior in terms of agreement with experimental results. [7]

Chapter 2: Method

To simulate BST systems, a first-principles-based effective Hamiltonian method was used, implemented as a Monte Carlo simulation coded in the FORTRAN programming language and run on a UNIX server. In this chapter, the author first presents a summary of the method in general, which was first presented in the author's maaster's thesis, *Modeling of Barium Strontium Titanate From First Principles.* [7] For a more detailed description of the underlying method, please refer to Chapters 3 and 4 of that work. The latter parts of this chapter will discuss modifications to the method necessary to model strained systems and thin-films.

1. The Basic Method

To model simple perovskites (such as pure $BaTiO_3$, designated BT) Zhong, Vaderbilt and Rabe [8] proposed a five-term effective Hamiltonian, given in Equation 4.

$$E = E^{dipl} + E^{short} + E^{elas} + E^{int} + E^{self}$$

Equation 4

Here, E^{dipl} is the long-range dipole interaction, E^{short} is all short-range dipole interaction, exclusive of any long-range dipole interaction, E^{elas} is the elastic energy (the energy cost of deformations to the crystal) and E^{int} accounts for the coupling between the elastic energy and the local dipoles [8]. More complete descriptions may be found in the author's Master's Thesis [7].

The remaining term, E^{self}, is of particular interest. It expresses the self-energy associated with the local dipoles at site *i*. As a Taylor expansion, this energy term can be expressed as given in Equation 5 [8]:

$$E^{self} = \kappa_2 + \alpha u_i^2 + \gamma\left(u_{ix}^2 u_{iy}^2 + u_{iy}^2 u_{iz}^2 + u_{iz}^2 u_{ix}^2\right)$$

Equation 5

The variable u_i is the local mode at site *i* associated with the lowest transverse-optical phonon mode, and in this case is centered on the B-sites. This quantity can be multiplied by the Born effective charge associated with the local mode to find the dipole moment. The constants κ_2, α and γ in Equation 5 are calculated from first-principles. However, such calculations make use of approximations, such as the Local Density Approximation, which can lead to simulated results which do not agree with experimentally found results. To correct this problem, it is suggested in papers by Tinte, et al. [38] and Akbarzadeh et al. [40] that one may modify the value of one or more of these constants to achieve results which do conform to those found experimentally. [2], [12]

The task of adjusting a chosen constant (in this case, the κ_2 constant of Equation 5) was the main focus of the author's Master's research project. A single case was chosen (a bulk $Ba_xSr_{1-x}TiO_3$ (BST) alloy with 50% Ba and 50% Sr composition) and κ_2 was adjusted until the highest-temperature transition (that is, the Curie Temperature) matched the transition temperature found experimentally [2], [12]. It was found that by matching only this single point, accurate results were achieved for not only the lowest-temperature transitions of the chosen BST system with 50% Ba composition, but for all

BST systems with a Ba concentration greater than 30%. [7] This process is highly analogous to an experimentalist calibrating his or her instruments before taking readings. The κ_2 value found to yield the closest agreement with experiment, and the value used for the research presented here, was $\kappa_2 = 0.064718$. [7]

The simple, five-term effective Hamiltonian is, as stated above, sufficient to model non-alloyed perovskite systems. However, to model alloyed systems, it is necessary to make use of a technique called Virtual Crystal Approximation (VCA). In VCA, the alloy is first treated as if it were made up of fictitious atoms whose properties are an average of those used in the alloying [41), (42] (in the present case, these atoms are Ba and Sr). Next, perturbation terms are added to (or subtracted from) the energy of the system depending upon which atom (Ba or Sr) is actually present at a given site. The resulting effective Hamiltonian is given in Equation 6 [43), (44]:

$$H\{(\mathbf{u_i}),(\mathbf{v_i}),\eta_H,\eta_{loc},\boldsymbol{\sigma_j}\} = H_{ave}\{(\mathbf{u_i}),(\mathbf{v_i}),\eta_H\} + \sum_{ij}\left[R_{j,i}\sigma_j\mathbf{f}_{ji}\cdot\mathbf{v}_i + Q_{j,i}\sigma_j\mathbf{e}_{ji}\cdot\mathbf{u_i}\right] + \frac{1}{2}\sum_i\sum_{l,\alpha,\beta}B_{l,\alpha,\beta}\eta_{loc,l}(i)u_{i,\alpha}u_{i,\beta}$$

Equation 6

In this equation, H_{ave} is the basic perovskite effective Hamiltonian, given in Equation 4, as calculated for the VCA "average crystal" whose properties are a mix of 50% Ba and 50% Sr for the A-atoms. It is a function of the local mode ($\mathbf{u}_i$), local displacement ($\mathbf{v}_i$) which is related to the inhomogeneous strain, and the homogeneous

strain, η_H. The remaining terms in Equation 6 represent perturbations about H_{ave}. $R_{j,i}$ and $Q_{j,i}$ are variables which relate to interactions arising in alloys, while $\mathbf{f}_{ji}$ is a unit vector which connects the A-atom site *j* to the A-origin of $\mathbf{v}_i$. Similarly, $\mathbf{e}_{ij}$ is a unit vector connecting the A-atom site *j* to the B-origin of $\mathbf{u}_i$. σ is the alloy configuration, and its elements (σ_j) are either +1 or -1 depending on whether site *j* contains a Ba or Sr atom, respectively. [43] [44] This configuration is stored in a file, "Alloy," which is read by the Monte Carlo program.

Note also that Equation 6 includes an alloy-induced strain η_{loc} which arises due to the difference in size between Ba and Sr atoms. [44] The shear-components of this strain are assumed to be zero. The remaining components of η_{loc} at a given B-site *i* are given by Equation 7 [44]:

$$\eta_{loc,11}(i) = \eta_{loc,22}(i) = \eta_{loc,33}(i) = \frac{\Delta a}{8a_{BST}} \sum_j \sigma_j$$

Equation 7

In Equation 7, the index *j* runs over the nearest A-site neighbor sites of site *i*. Also, a_{BST} is the lattice constant of the VCA alloy, and Δa is the difference between a_{BST} and the lattice constant of pure BT. The total strain of the system is now therefore given by Equation 8:

$$\eta = \eta_H + \eta_{loc} + \eta_I$$

Equation 8

The generalized effective Hamiltonian of Equation 6 and the alloy-induced strain of Equation 7 were used in a Monte Carlo program capable of simulating bulk BST systems (such as those examined during the author's Master Thesis research [7]) and graded BST systems. The program generates a random number and makes a "test step," changing one degree of freedom (u_i, v_i, or η_H). The resulting energy change of the step is then calculated; if the net change is negative, the change is saved, but if not it is rejected, unless another random number is less than $e^{\Delta Energy / k*T}$, where k is Boltzmann's constant and T is the temperature in Kelvin. When studying the systems examined in this dissertation, this process is repeated for each degree of freedom for each site a total of 400,000 times at a given temperature.

To correct for the fact that the Local Density Approximation method consistently underestimates the lattice constant of the system, an artificial, constant negative pressure was applied to the simulated system. The change in overall energy due to this pressure is given by Equation 9 [45]:

$$E_{pres} = a^3 p\left[\eta_{H,1} + \eta_{H.2} + \eta_{H,3}\right]$$

Equation 9

Here, p is the value of the applied pressure, and a is the lattice constant at 0K. As the desire was to decrease the overall energy of the system (thereby slightly expanding the overall lattice constant) this applied pressure was negative, and had a value of -5.2 Gpa. Note that the only difference between bulk and graded cases was the content of the "Alloy" input file, and no modification to the code itself was necessary.

To create a graded supercell, smaller blocks of data each describing a single crystal layer with a given composition were copied and pasted together to create the complete supercell as stored in the Alloy file. The size of the supercell in the x-and y-directions was 12 B-sites * 12 B-sites, but the size of the z-direction was determined by the system being modeled. The rules were that there must be an equal number of A-layers of each unique Ba composition the researcher selected to use in the grading, and that the compositions were selected to yield an overall average composition of 70% Ba (meaning 30%Sr). The second requirement dictated that two-tiered grading will involve the compositions 40% Ba and 100% Ba (pure BT), three-tiered grading involved 40%, 70% and 100% Ba, and so forth. The first requirement dictated the size of the model supercell in the z-direction. For example, in a three-tiered (40/70/100) system with a region thickness (n) of five, there must be a total of 3*5 or 15 layers along the z-direction in order to comply with the second requirement. For n=6, the z-direction would then become 18 layers thick, and so forth. The entire supercell is then periodically repeated by the program in all directions for bulk materials.

2. Systems With Epitaxial Strain

The next step was to model graded systems experiencing an epitaxial strain (i.e., a strain that arises from the material of interest residing on a substrate). This was achieved by "freezing" the strain such that the in-plane (x and y) lattice parameters were forced to match the lattice parameter of the substrate. The substrate chosen for these simulations was pure Strontium Titanate ($SrTiO_3$), which has a lattice parameter of a_{ST} = 7.364897 Bohr (according to the effective Hamiltonian approach used in this work).

In order to match lattice parameters, it was necessary to find a way to balance Equation 10 for each B-layer *i*:

$$[1 + \eta_H + \eta_{loc}(i)]a_{BST} \neq a_{ST}$$

Equation 10

In Equation 10, a_{BST} is the equilibrium lattice constant of the VCA alloy. Also, η_{loc} is the alloy-induced strain at a given B-layer, *i*. It would be convenient if the left-hand side of Equation 10 gave the same lattice constant (namely, a_{ST}) for each layer, but that was not possible because the lattice constant of a given B-layer depended on the value η_{loc} of that layer. The value of η_{loc} depended on the average composition around this given layer, which will by definition not be constant throughout the material in a graded system. Therefore, the equation was balanced by introducing a term to the left-hand side of Equation 10, denoted $\eta_{INHO,}$ to correct for this composition-induced variation. This new correcting term had to be calculated for each layer interface in the system. The new, balanced equation which resulted is Equation 11:

$$[1 + \eta_H + \eta_{INHO}(i) + \eta_{loc}(i)]a_{BST} = a_{ST}$$

Equation 11

In order to find η_{INHO} from Equation 11 it was necessary to find the values of $\eta_{loc}(i)$ and $\eta_{H.}$ $\eta_{loc}(i)$ was found using Equation 12:

$$\eta_{loc}(i) = \frac{\Delta a}{a_{BST}}(2\chi(i) - 1)$$

Equation 12

In Equation 12, $\chi(i)$ is the average composition of the two A-layers sandwiching B-layer *i*. Δa and a_{BST} are the same as described above for Equation 7. The value of the ratio of Δa and a_{BST} was 0.01087.

Typically, the homogeneous strain η_H is defined by the following equation, Equation 13:

$$\eta_H = \frac{a_{lat} - a_{BST}}{a_{lat}}$$

Equation 13

Here, a_{lat} is the equilibrium lattice constant assumed by the system, but this was not originally known. Therefore, for practical purposes η_H was initially calculated using Equation 14:

$$(1 + \eta_H + \eta'_{loc}) * a_{BST} = a_{ST}$$

Equation 14

In Equation 14 the term η'_{loc} is the average alloy-induced strain through the whole system, which was found using a modification of Equation 12, now dubbed Equation 15:

$$\eta'_{loc} = \frac{\Delta a}{a_{BST}}(2\chi' - 1)$$

Equation 15

In Equation 15, χ' is the average composition of the whole system, which is .7 (70% Ba) for all systems considered in this work.

Comparing Equation 11 and Equation 14, it is seen that

$$\eta_{INHO}(i) + \eta_{loc}(i) = \eta'_{loc} \rightarrow \eta_{INHO}(i) = \eta'_{loc} - \eta_{loc}(i)$$

Equation 16

Equation 16 provided the most practical means to calculate η_{INHO}. For purposes of the simulation, the values of $\eta_{INHO}(i)$ were stored in a new input file, StrainINHO, which was read by the modified FORTRAN code and used when calculating the strain-based degree of freedom in each computational cycle. Equation 14 and Equation 15 were then used to find η_H, and the description of epitaxial conditions was thus completed.

3. Thin-Films

For the modeling of thin-films, it was necessary to make several changes to the basic simulation.

The basic simulation repeats the input supercell periodically in all directions. Therefore, in order to model a thin-film, it was first necessary to remove this periodic repetition in the z-direction. When doing so, it was important that the material terminated

on an A-layer at both top and bottom, to mimic A-O terminated surfaces. Further, the notation in the Alloy input file was modified to allow the user to indicate whether the material is bounded on either side by a vacuum or a substrate. Outside of the material, local modes, displacements and strains were set to zero.

The electrical boundary conditions also had to be taken into account when simulating a thin-film. If the boundary conditions reflect an ideal short-circuit (SC) then no charge will build up at the boundaries and polarization along the growth-direction is favored. In this case, the dipole interaction will, in fact, be identical to that of a three-dimensional system. [26] The dipole-dipole interaction matrix (denoted Q-matrix) for such a system is given by Equation 17 [26]:

$$Q^{3D}_{\alpha,\beta,i,j} = \frac{4\pi}{V}\sum_{G\neq 0}\frac{1}{G^2}e^{\frac{-G^2}{4\lambda^2}}G_\alpha G_\beta \cos\left(G\cdot r_{ij}\right) - \frac{4\lambda^3\delta_{\alpha\beta}\delta_{ij}}{3\sqrt{\pi}}$$

Equation 17

In Equation 17, V is the cell volume, G represents reciprocal lattice vectors, λ is the Ewald parameter, r_{ij} is the vector connecting site i to site j and δ_{ij} is the Kronicker symbol. [26] By contrast, the Q-matrix for a two-dimensional system under ideal open-circuit (OC) conditions is expressed in Equation 18 [26]:

$$Q^{2D}_{\alpha,\beta,i,j} = \frac{2\pi}{A}\sum_{G}\left\{G\cos(G\cdot\rho_{ij})\left[\frac{1}{\sqrt{4\pi}}\Gamma\left(-\frac{1}{2},\frac{G^2}{4\lambda^2}\right)\delta_{\alpha z}\delta_{\beta z}+\frac{1}{G^2}\operatorname{erfc}\left(\frac{G}{2\lambda}\right)G_\alpha G_\beta\right]\right.$$
$$\left.+\,Ge^{-G|z_{ij}|}\left[\left(\frac{G_\alpha G_\beta}{G^2}-\delta_{\alpha z}\delta_{\beta z}\right)\cos(G\cdot\rho_{ij})-\frac{G_\alpha\delta_{\beta z}}{G}\sin(G\cdot\rho_{ij})\frac{z_{ij}}{|z_{ij}|}\right]\right\}$$
$$-\frac{4\lambda^3\delta_{\alpha\beta}\delta_{ij}}{3\sqrt{\pi}}$$

Equation 18

In Equation 18, A is the area of the supercell, r_{ij} is the same as in Equation 17, z_{ij} is the projection of r_{ij} onto the z-axis, and ρ_{ij} is the projection of r_{ij} onto the x-y plane. Also, Γ is the incomplete gamma function.[26] All other parameters are the same as described for Equation 17. Under these conditions, charges will build up at the boundaries of the material if the polarization lies along the z-direction. This creates a so-called depolarizing field, which acts to annihilate this polarization along the z-direction. Therefore, under this boundary condition, polarization in the x-y plane is favored.

For a given system, the dipole interaction energy may then be found using Equation 19[26]:

$$E_{dip} = \frac{1}{2V}\sum_{\alpha\beta ij} Q_{\alpha\beta ij}p_\alpha(r_i)p_\beta(r_j)$$

Equation 19

Here, Q is whichever interaction matrix is appropriate to the system, and the p terms are the dipole moments involved in the interaction (which are directly related to the

local modes). Further, i and j are sites in the supercell, and α and β run over the Cartesian coordinates.

For practical purposes of the simulation, the user may modulate smoothly between these two cases by "screening" the depolarizing field, as described, e.g., in Bin-Omran et al. [25] The maximum depolarizing energy per volume is the difference in energy between the perfect OC conditions and perfect SC conditions, as expressed in Equation 20 [26]:

$$\langle E_{dep} \rangle = \frac{1}{2V} \sum_{\alpha\beta ij} \left[Q^{2D}_{\alpha\beta ij} - Q^{3D}_{\alpha\beta ij} \right] p_\alpha(r_i) p_\beta(r_j)$$

Equation 20

To implement the screening of this field, a parameter β was introduced in the simulation program, and it indicated the degree of compensation for the depolarizing field. The values ranged between 0 and 1, where β =0 indicated an open-circuit condition, while β=1 implied a short-circuit. The overall effective Hamiltonian used in the simulation is therefore shown in Equation 21 [25]:

$$H_{tot} = H_{eff} + \frac{1}{2} \beta \sum_i \langle E_{dep} \rangle \cdot Z^* u_i$$

Equation 21

Here, H_{eff} is the effective Hamiltonian for the bulk system, as given in Equation 6, except that the dipole-dipole interaction term is based on the Q-matrix of Equation 18 rather than that of Equation 17 [25].

Chapter 3: Results

Here are presented the results gained by using the methods described in Chapter 2. Systems with two, three, and five-tiered grading and compositionally graded systems with layer thicknesses of n=1 to n=8 were modeled. Results for unstrained systems are presented first, followed by the results found for systems under epitaxial strain. Finally, exploratory results for thin-film systems are also presented.

1. Unstrained Graded Systems

A. Two-tiered (40/100) Systems

For the case of $(Ba_{0.4}Sr_{0.6})TiO_3$ alternated with pure $BaTiO_3$ (which is denoted as 40/100 or two-tiered grading) the behavior of the components of the local modes with changing temperature was first examined for a given layer thicknesses (n). An example of such a graph is given in Figure 7.

In this figure, note that at high temperatures all components were zero, indicating no displacement from an equilibrium paraelectric phase (denoted as C). As temperature decreased, first one component increased (denoted as T) then two (denoted as O) then finally all three components were greater than zero and equal to one-another (denoted as R). This was the same pattern of transitions observed in bulk material. The case displayed in Figure 7 has n=2. However, it should be noted that, for the case of n=1, the transition temperatures were equal to those of the bulk material with 70% Ba composition.

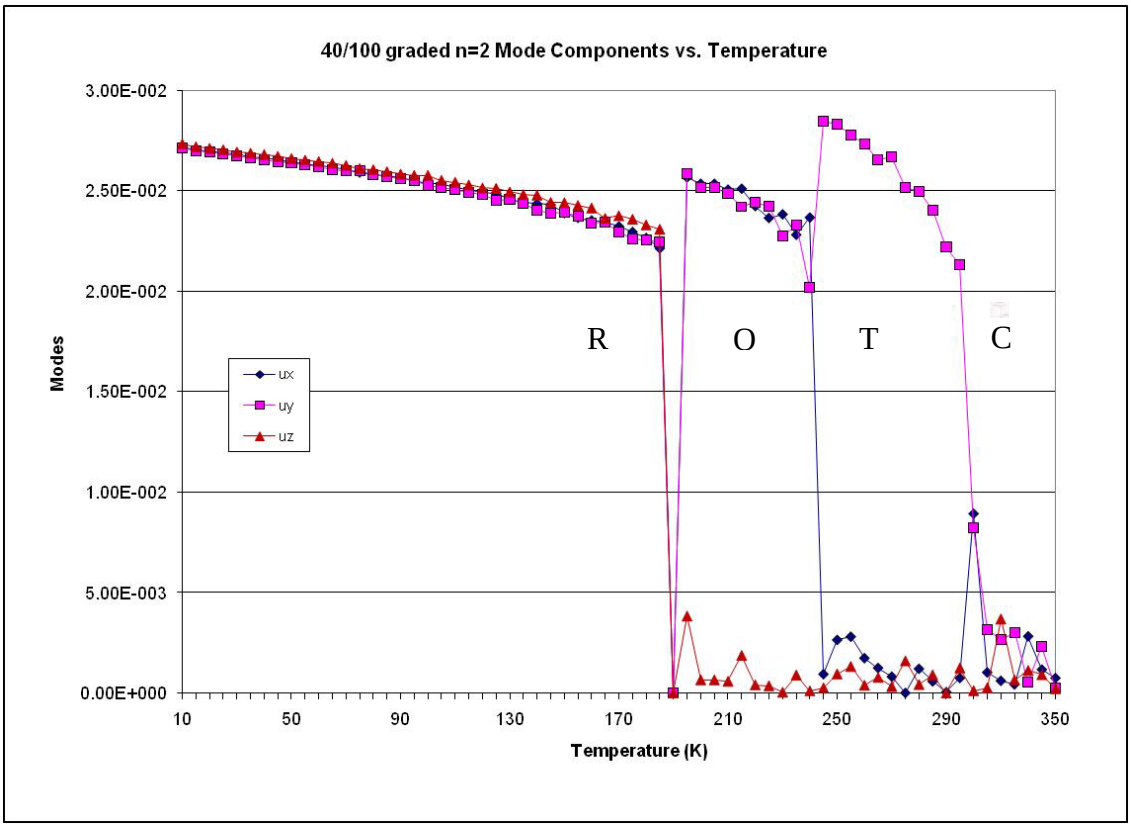

Figure 7: the components of the local modes changing with temperature, for 40/100 system with n = 2.

In all mode versus temperature graphs, such as Figure 7, u_1 is the greater of u_x or u_y, and u_2 is the lesser of these values. The data was displayed in this manner in order to enhance clarity, because the symmetry states which occur do not depend on which components are greater than zero, but only how many are greater than zero.

For larger n ($n \geq 4$), two distinct types of behavior are seen; with domain stripes, and without domain stripes. When the simulated superlattice held only *one* period (eg, for n=5, there are 5 layers of $(Ba_{0.4}Sr_{0.6})TiO_3$ followed by 5 layers of pure BT *once*) no domain stripes were present. In these cases, the behavior of transition temperatures versus period (n) is illustrated in Figure 8:

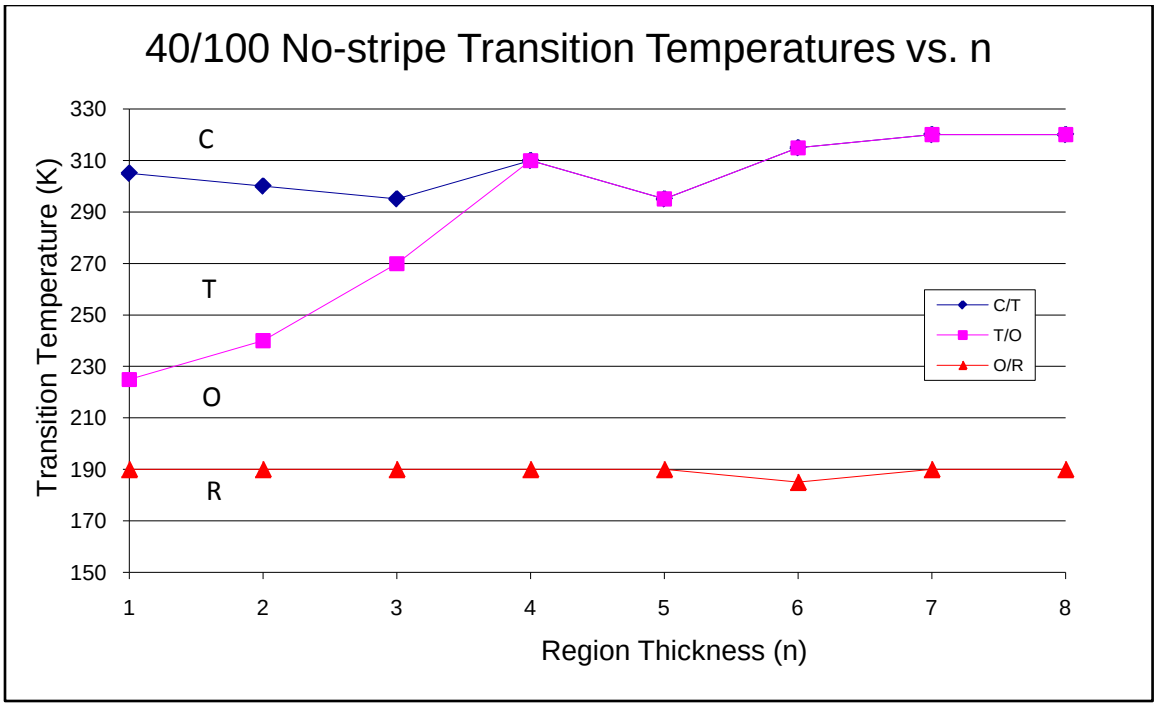

Figure 8: Transition Temperatures (C/T, T/O, O/R) as a function of layer thickness (period, n)

For low n (n=1,2,3) it was observed that the temperature of the T-to-O transition increased, until it merged with the C-to-T transition, merging into a single C-to-O transition for n=5 and above. Evidence that the transitions actually merged is given in Figure 9. Recall that the final results of a Monte Carlo simulation are an average over many repetitions. Figure 9 charts the percentage of repetitions displaying each symmetry type (T, O and R) plotted against temperature (n=6 is used as an example):

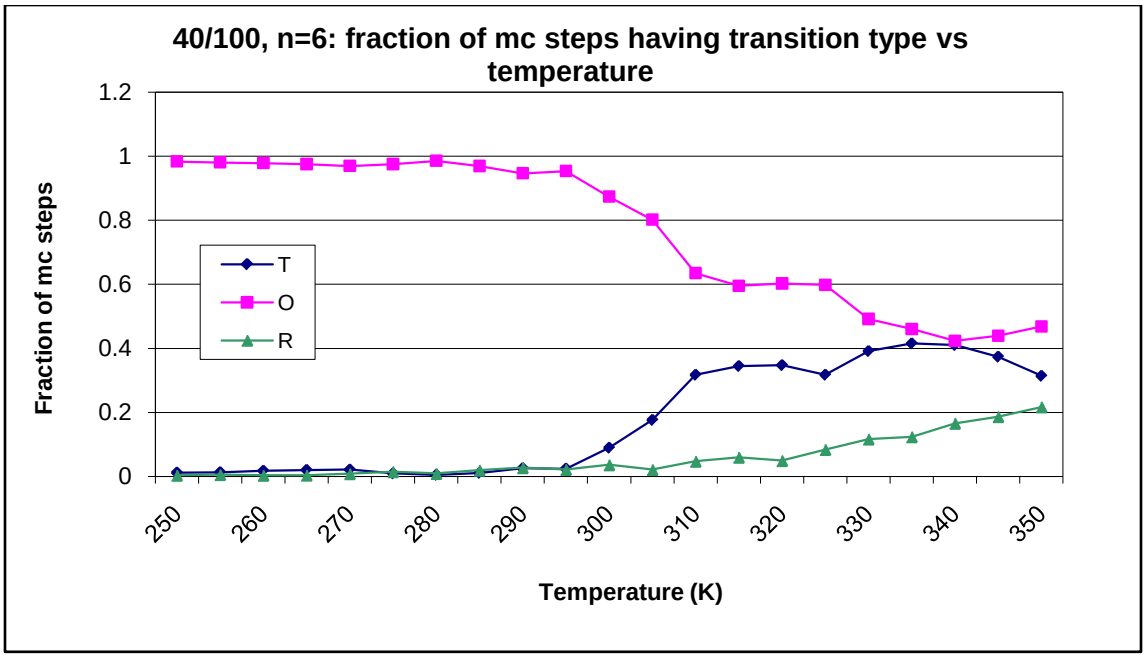

Figure 9: fraction of the 400,000 monte-carlo steps displaying given trasition types, versus temperature, for 40/100 n=6

This merging of transitions was most clearly seen by comparing the mode versus temperature behavior of the n=3 superlattice and the n=5 superlattice. The n=3 graph still showed a distinct region of T-phase, but the n=8 graph showed two components of the local mode increasing simultaneously.

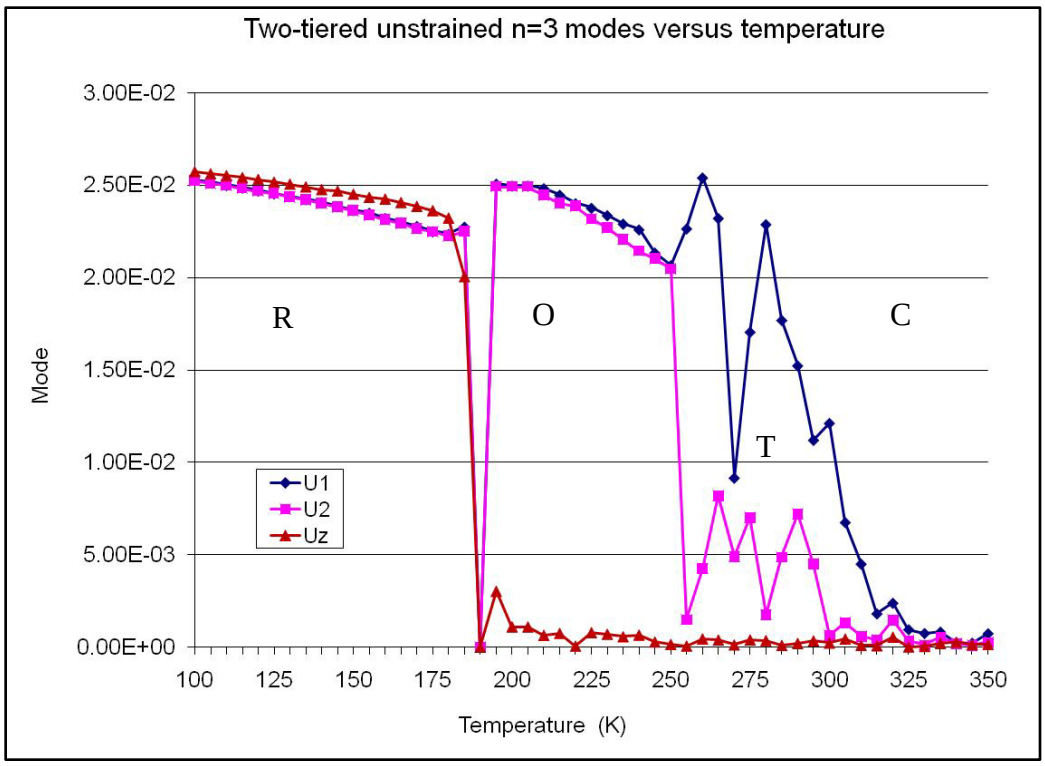

Figure 10: mode versus temperature behavior for n=3 superlattice (two-tiered system)

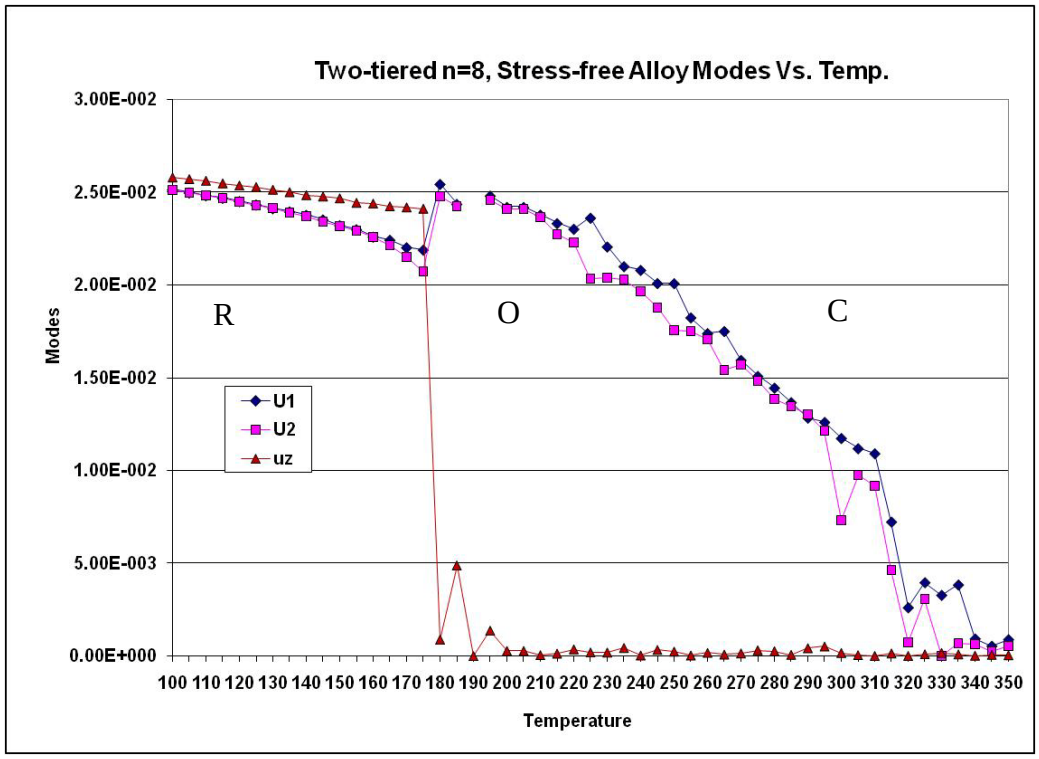

Figure 11: Mode versus temperature behavior for n=8 superlattice (two-tiered system)

To understand why this merging of transitions occurs, it was necessary to examine the response of each layer of the simulated system. It was especially instructive to compare the layer-by-layer response of a small-n system with a large-n system for a given temperature. To this end, the n=3 and n=8 cases for T=285K are shown below in Figure 12 and Figure 13. The layer index indicates the B (Ti-O) layer which lies at the interface of each pair of alloyed (Ba-O/Sr-O) A-layers.

Notice that, for n=3 (Figure 12), all layers have two components of the local mode equal to zero, and one component greater than zero in all layers, though the response is slightly weaker in the Sr-rich layers. This indicated that the whole material was responding more-or-less homogeneously, rather than as a strict sum of its parts.

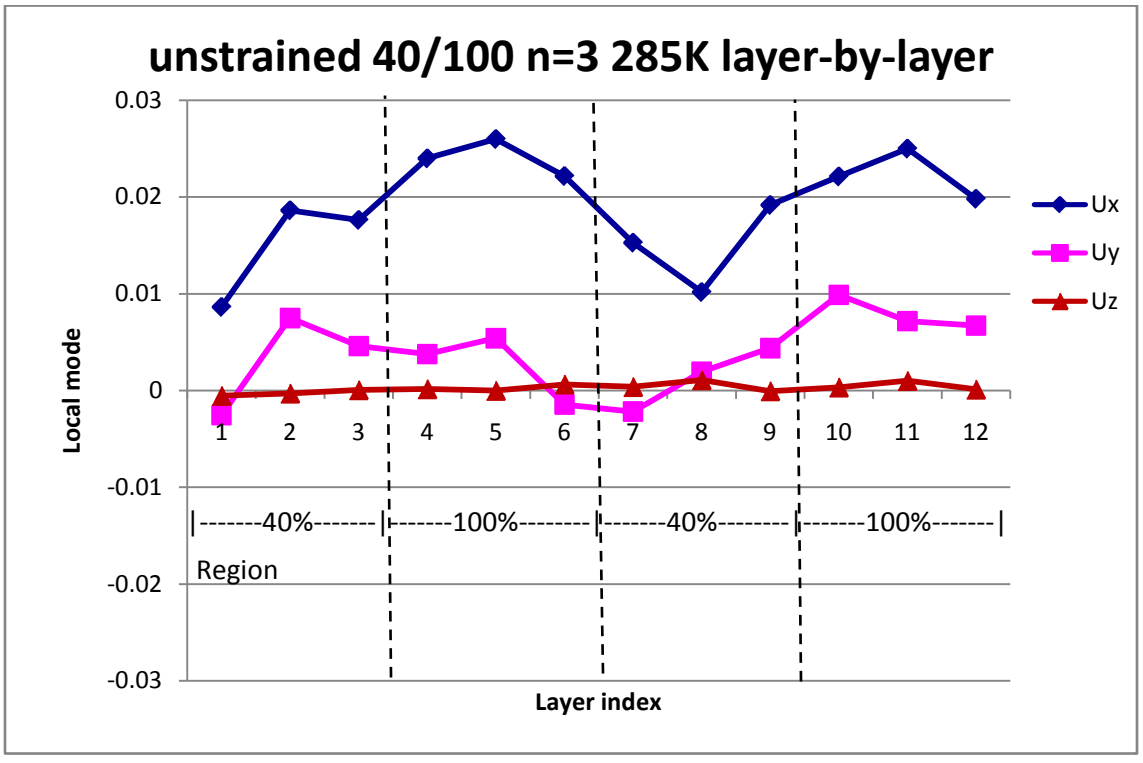

Figure 12: layer-by-layer response of 40/100 n=3 at 285K. The regions are labeled by their composition in % of Ba.

By contrast, in the n=8 case (Figure 13), the BT-layers showed O-type symmetry ($u_x = u_y \neq 0$, $u_z = 0$), while the Sr-rich layers still showed C-type symmetry. Each compositional block was independently responding as it would in bulk at the given temperature. Therefore, the overall material showed an average symmetry of O. This behavior (homogeneity at small n, independent response at large n) was consistent with the findings of others, such as Sepilarsky et al. [30] and Lisenkov and Bellaiche [46].

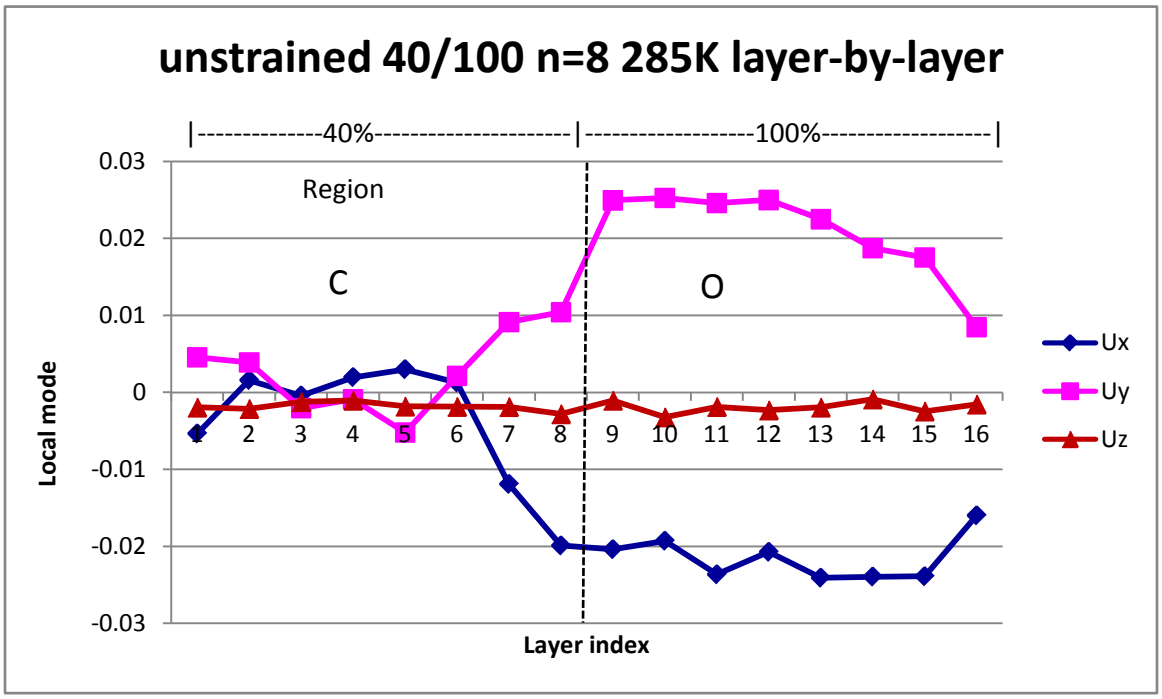

Figure 13: layer-by-layer response of 40/100 n=8 system at 285K

When the simulated superlattice contained two or more periods (e.g., to continue the initial example, take 5 layers of $(Ba_{0.4}Sr_{0.6})TiO_3$, 5 layers of BT, then 5 more layers of $(Ba_{0.4}Sr_{0.6})TiO_3$ and 5 more of BT such that the previous supercell is, in effect, doubled) domain stripes can appear. When domain stripes occur, the mode versus

temperature graph usually looked like the plot in Figure 14, with the x or y component dropping to zero just as the z-component increases (n=5 case, used as example):

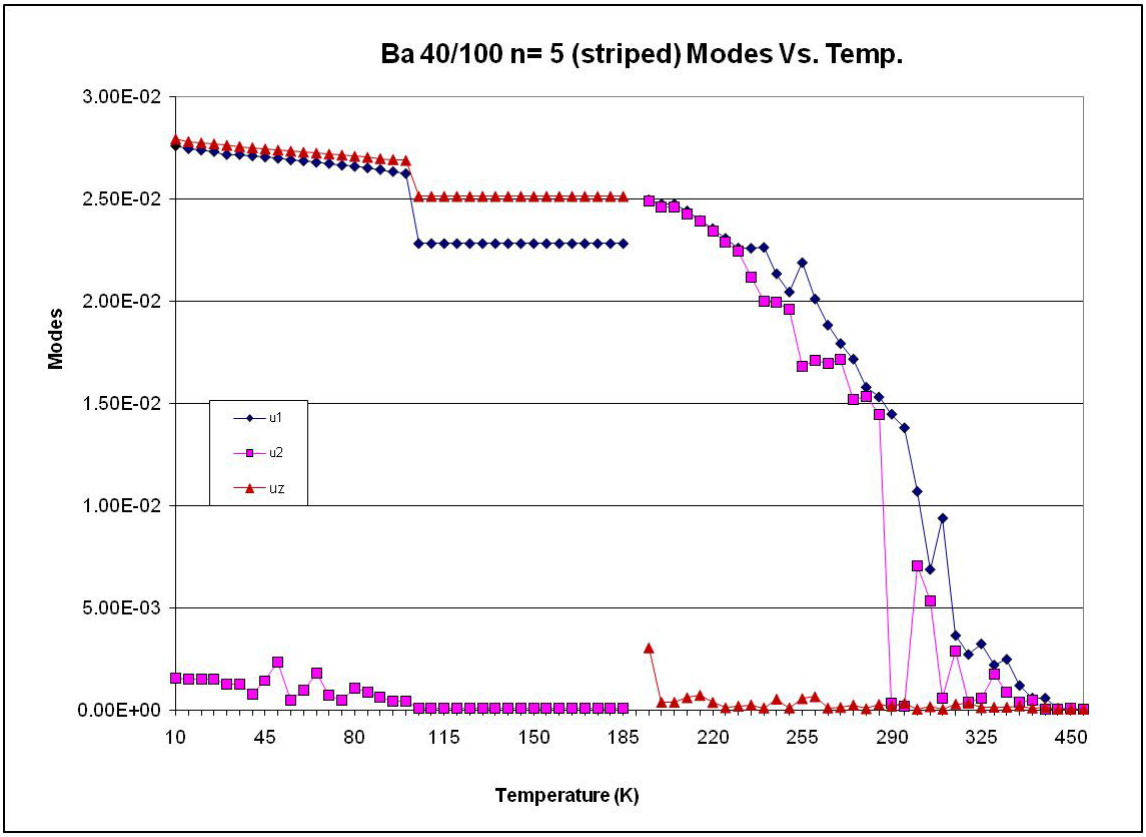

Figure 14: Mode components versus temperature, for doubled 40/100 n=5

Because the mode components were averages over the whole supercell, they could become zero in one of two ways: the local mode at each site could have been near zero, or approximately equal numbers of sites could have been (+) or (-) a given magnitude, respectively. This second possibility was the case when there were domain stripes, a phase which is denoted D. Evidence that the one mode-component of the current system was zero due to domain striping, not an otherwise-unknown transition was

found when looking at the average mode by layer at low temperature, as shown in Figure 15 (again, n=5, at 10K):

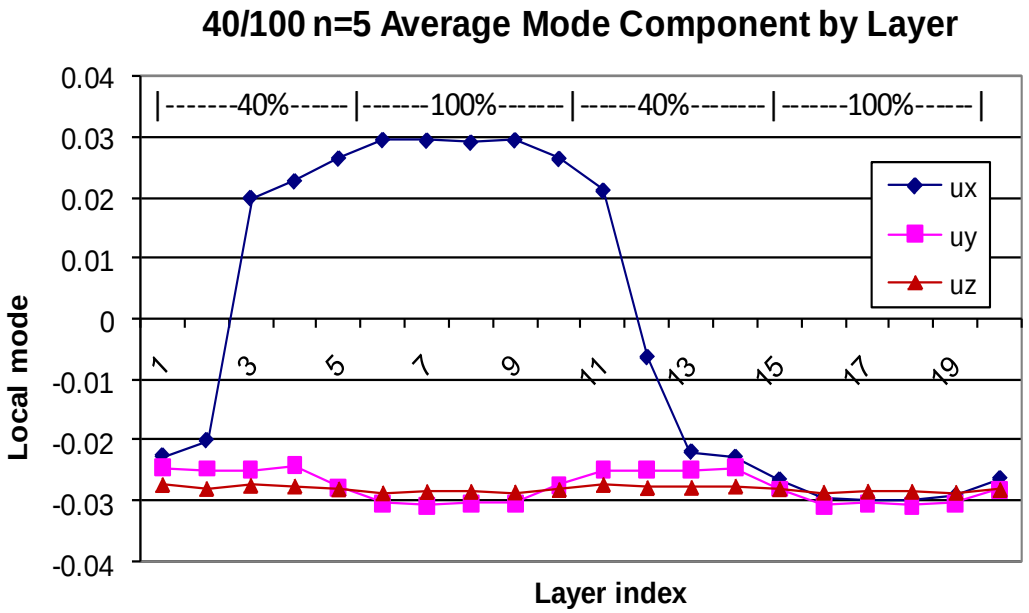

Figure 15: Average magnitude of mode components in each crystal layer (Temperature of 10K)

The above pattern (positive displacement in one region and negative displacement in the other) resulted in the following domain picture, which most clearly illustrated the striped domains (see Figure 16). Note that each stripe was approximately half the height of the simulated material in the growth direction (z-axis). That is, one set of $Ba_{0.4}Sr_{0.6}TiO_3$/BT layers possesseed a negative dipole moment along the x- (or equivalently, y-) axis, and the second set of $Ba_{0.4}Sr_{0.6}TiO_3$/BT layers possesseed a positive dipole moment.

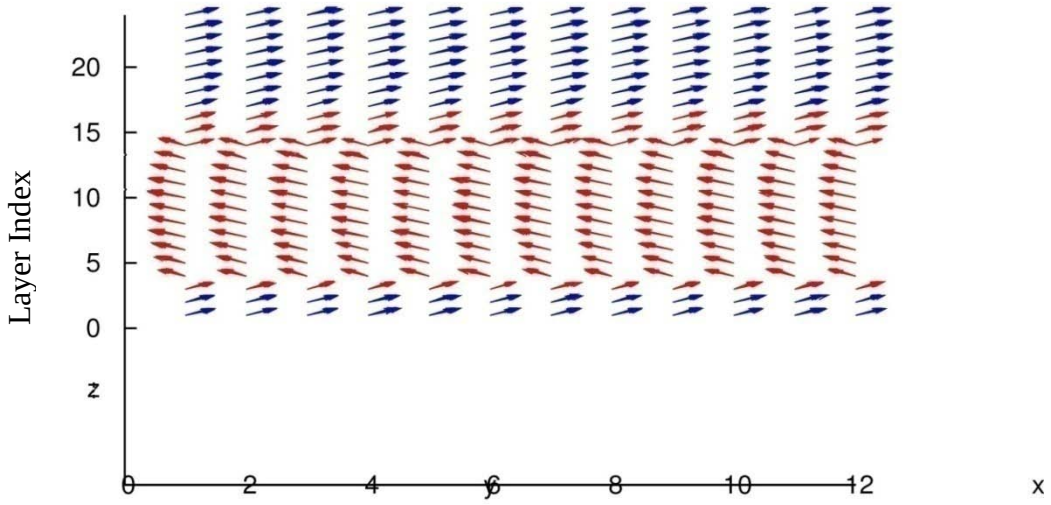

Figure 16: Image showing striped domains. Horizontal is either x- or y-axis, vertical is z-axis of crystal. 40/100 graded, n=4 case (unstrained). Blue Arrows indicate a positive x-component of the dipole moment, red indicates the negative of the same.

For systems with a doubled period, Figure 17 displays the behavior of transition temperatures versus region thickness (n) which was found. For 40/100 grading, striping was found at n=4 and above except for the n=8 case, which did not exhibit striping. It is possible that a new domain pattern was about to emerge if n had been increased further. This is one possible avenue of future investigation.

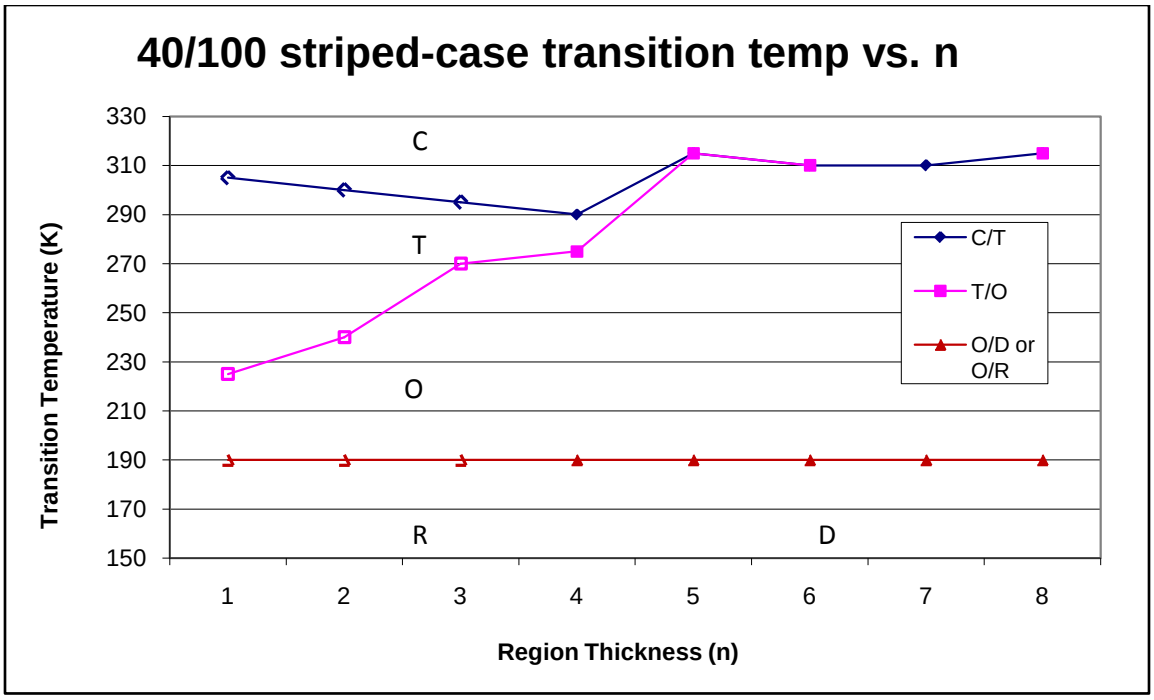

Figure 17: Transition temperatures versus period (n) for doubled (striped) cases. Open markers indicate small-n cases in which striping never appears.

When total energies per atomic site were compared between the two cases (striped and non-striped), the case without stripes was found to have the lower energy in the majority of cases. As a typical example, in systems of n=6 the case displaying domain striping had a total energy of -0.00270592 Hartree per atomic site, while the monodomain case had a total energy of -0.00272753 Hartree per atomic site. The local mode self-energy and elastic energy components tended to favor stripes, while the remaining components favored the simpler case. This was qualitatively consistent with results found elsewhere by Fu and Bellaiche. [10] At n=7, the total energy and the various components were extremely close in value between striped and non-striped cases, and at n=8 the short-range energy became favorable to stripes and in that instance the striped case was actually lower in energy. This was, however, a sole exception.

Finally, it is noted that, in non-striped cases, the x and y components of the mode sketch a sinusoidal curve when charted by layer (see Figure 18, with n=3):

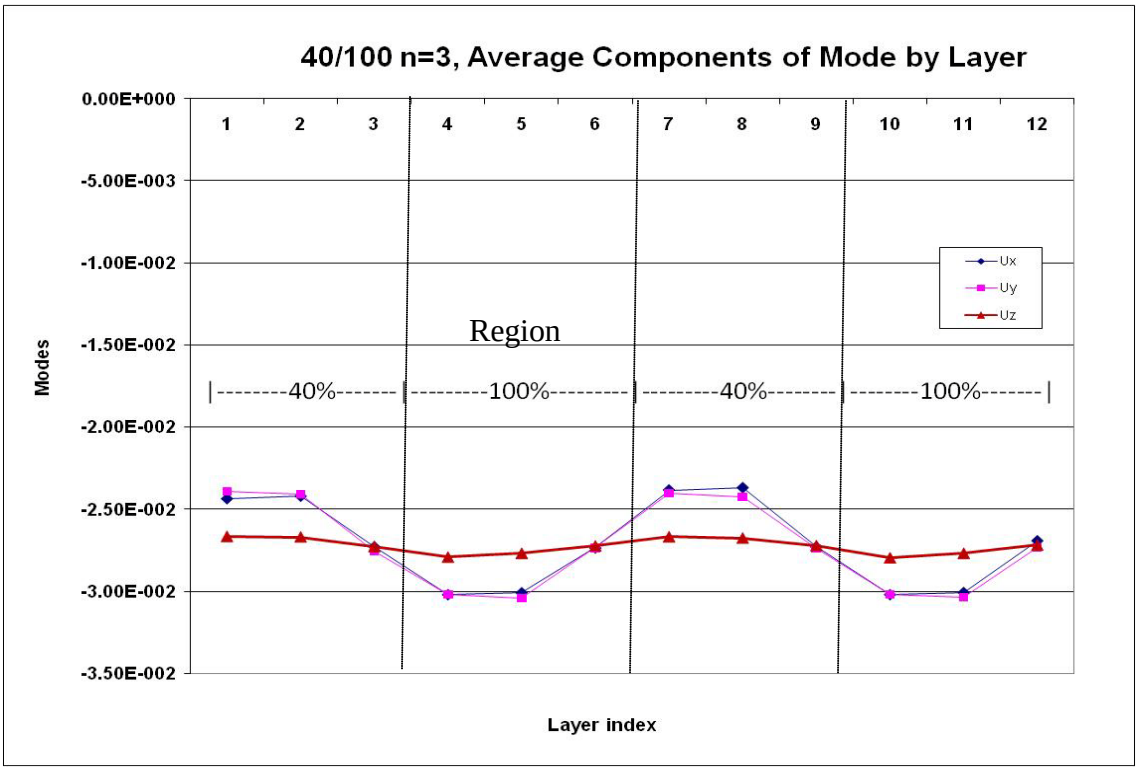

Figure 18: the components of the local mode, averaged by layer for 40/100 n=3 at 10K

Recall that the layer index marks the B (Ti-O) layers of the system. Also, though the amplitude of the variation is much smaller, the z-component also has a sinusoidal shape when averaged and charted by layer (see Figure 19).

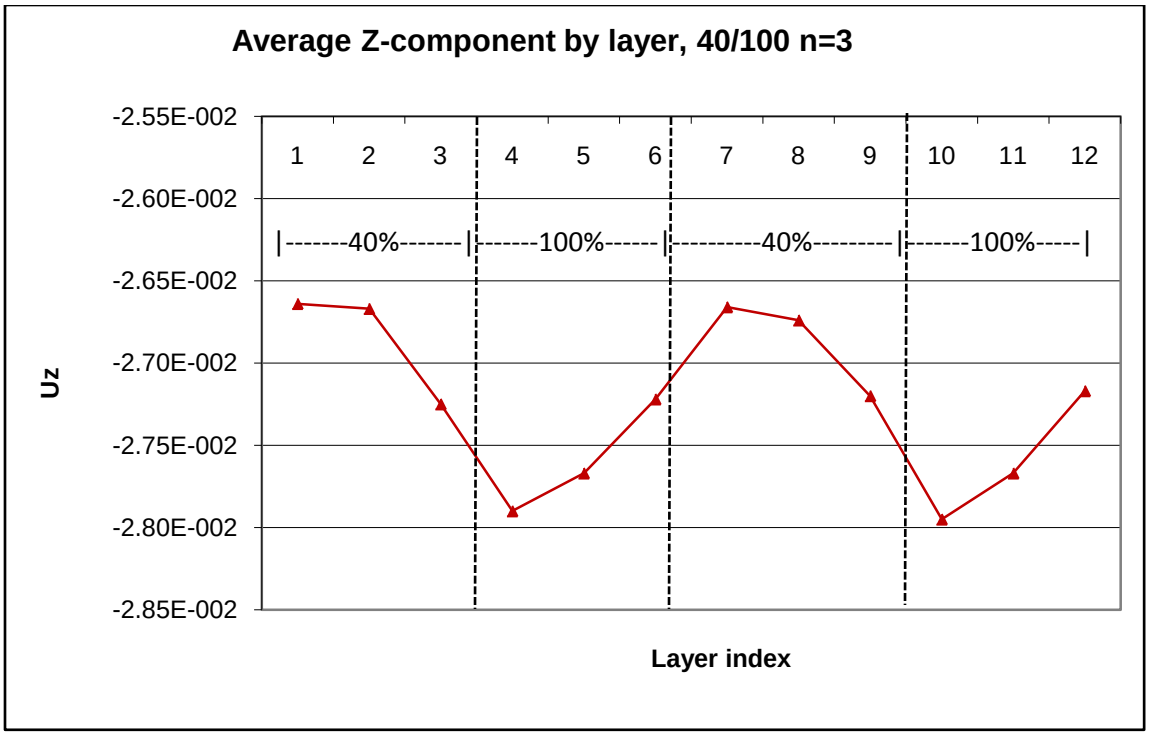

Figure 19: The z-component of the mode, averaged by layer (again, 40/100 with n=3 at 10K)

B. Three-tiered (40/70/100) Systems

Unstrained systems with three-tiered grading (recall that this includes regions of 40% Ba, 70% Ba and 100% Ba compositions) showed some behavior that was similar to the 40/100 systems, but other behavior that differed. The striped-domain behavior first appeared at n=3 for this system of grading, rather than at n=4 in the 40/100 case. However, the appearance of the stripes was still similar to Figure 16, and the striping still involved the x- or y-component of the dipole moments. Also, the single-domain cases of three-tiered systems had lower energy than the striped domain cases of the same n, the same as was found in 40/100-graded systems. This was the first indication that the

simulations predicted two local energy minima, close but distinguishable, leading to two possible meta-stable states in simulated systems (ie, striped and non-striped).

The primary difference between the two-tiered and tree-tiered systems appeared at higher values of n, where a possible monoclinic phase began to appear. Shown below in Figure 20 is a three-tiered system with n=6. The region of interest occured between about 275K and 250K, where two components of the local mode appear to be non-zero, but not equal to one-another (the apparent monoclinic phase).

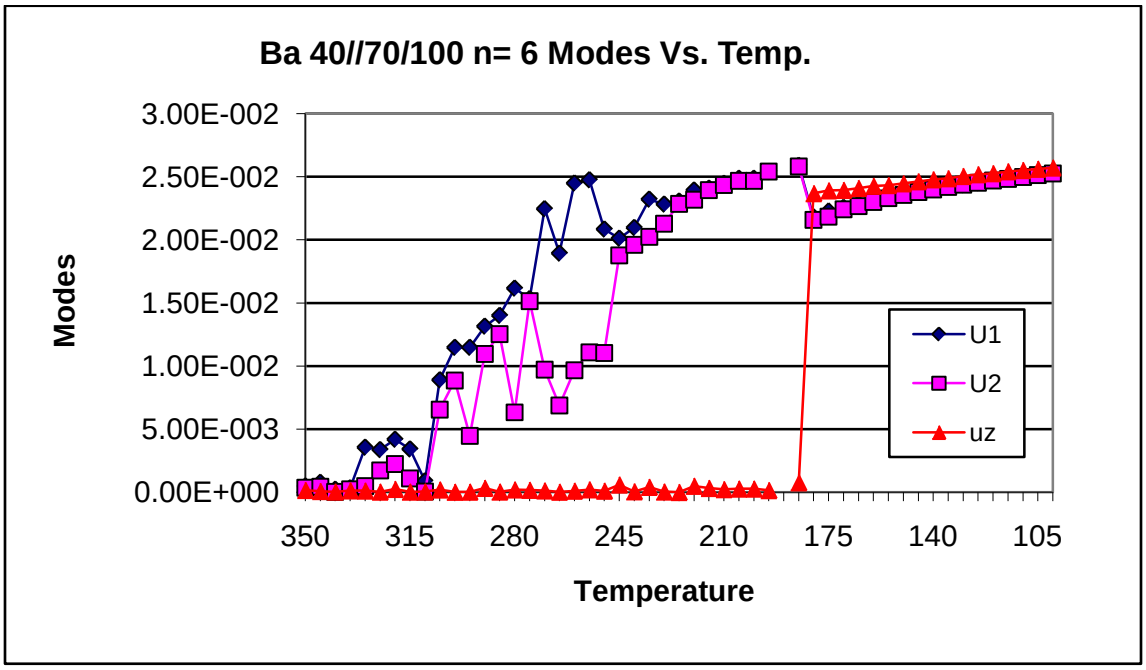

Figure 20: Three-tiered grading with n=6. Note the region between approximately 275K and 250K, displaying possible monoclinic phase.

Overall, the behavior of transition temperatures versus layer thickness (n) for the monodomain case is shown in the following figure, Figure 21:

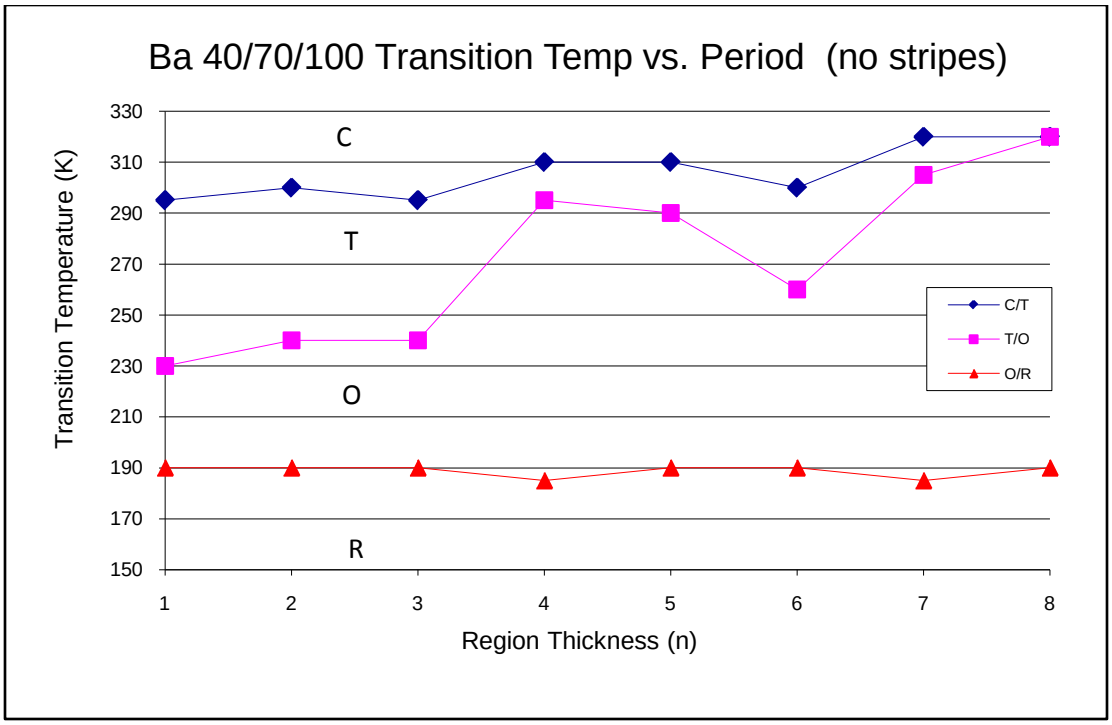

Figure 21: Transition temperatures versus layer thickness (n) for three-tiered, unstrained systems.

Like the two-tiered systems, the tetragonal-to-orthorhombic phase transition increases in temperature and approaches the cubic-to-tetragonal transition. In the case of three-tiered grading, this begins to occur at n=4. Some separation remains between the first two transitions, however, possibly due to the emergent monoclinic phase as shown in Figure 20.

C. Five-tiered (40/50/70/90/100) Systems

When the graded system included layers of five different compositions, further changes in behavior became apparent. For n of 5 or greater, a monoclinic phase appeared (as seen in three-tiered grading). At n=8, this monoclinic phase was also associated with the appearance of striped domains (shown in Figure 23).

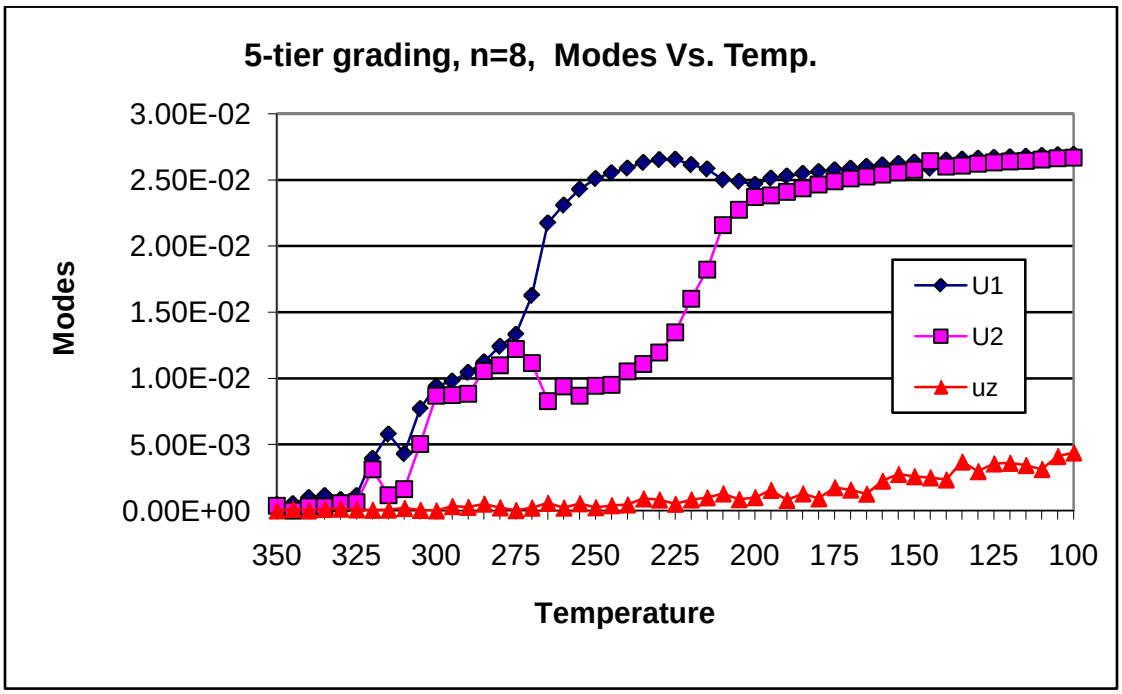

Figure 22: Five-tiered system with n=8. Monoclinic phase exists between 275K and 215K.

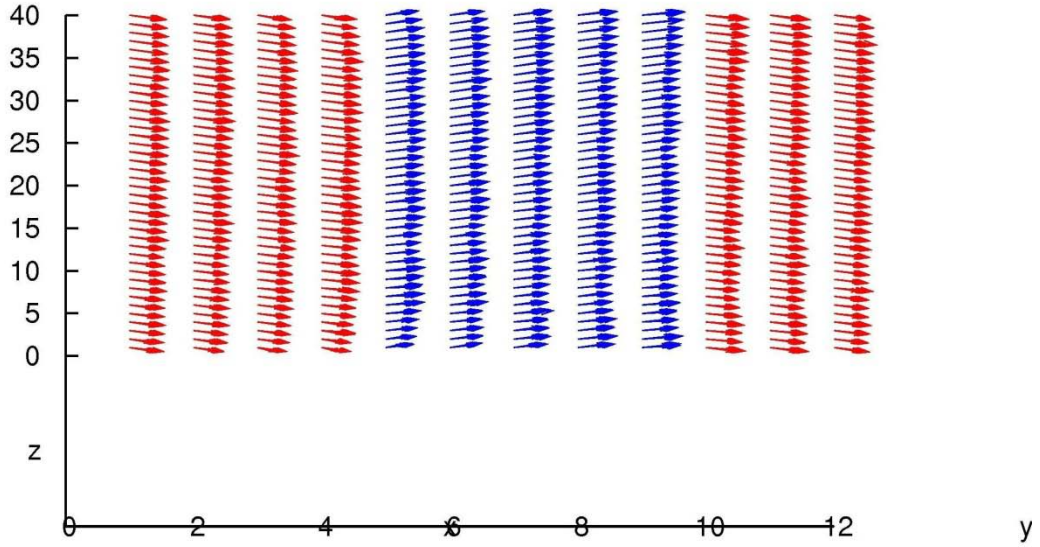

Figure 23: Striped domains seen in five-tiered n=8 system below 215K. Note the vertical orientation.

Unlike the striped domains found in two-tiered and three-tiered cases, these had vertical boundaries, and involved the z-component (rather than x- or y-component) of the dipole moment. Striped domains of this form are generally adopted by systems because doing so minimizes the depolarizing field effect which arises between the regions of differing composition.

To further understand the appearance of the monoclinic phase in Figure 22, it was once again useful to examine the layer-by-layer response of the system. The response of the 5-tiered, n=8 system at 300K is shown in Figure 24 and the response of the same system at T=250K is shown in Figure 25:

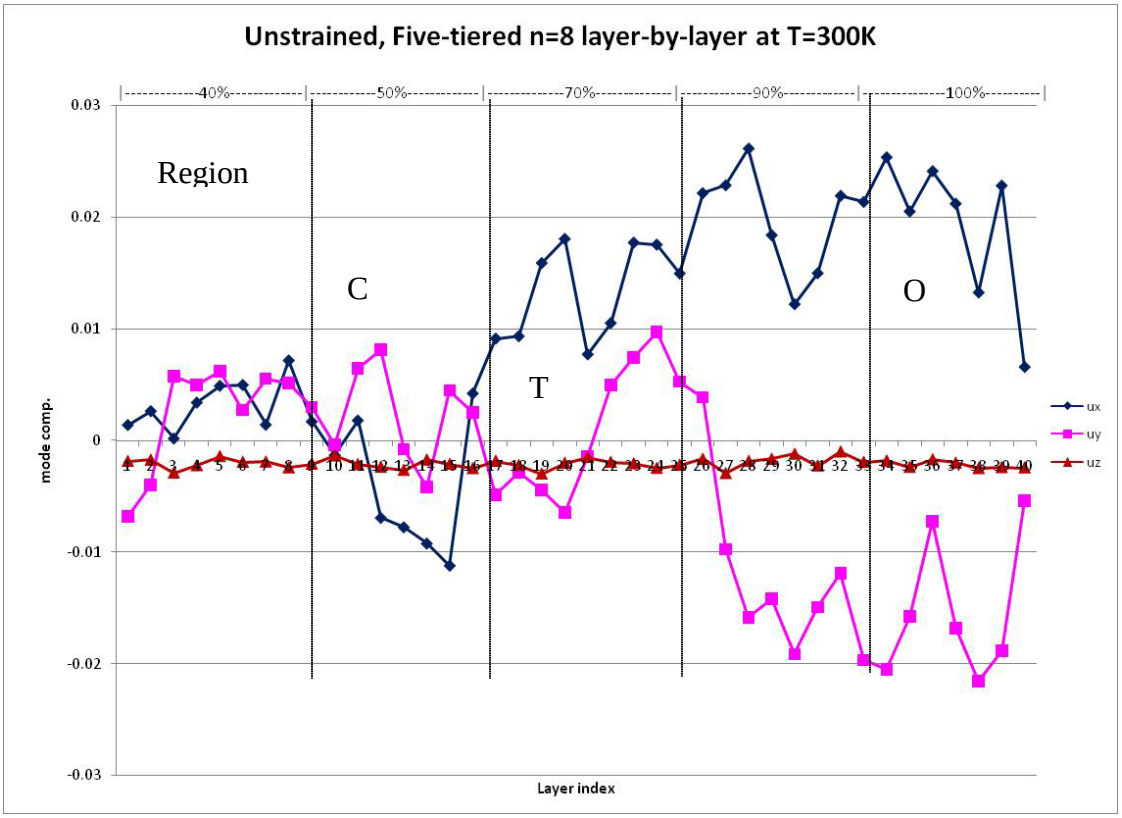

Figure 24: Layer-by-layer response of 5-tiered, n=8 at T=300K

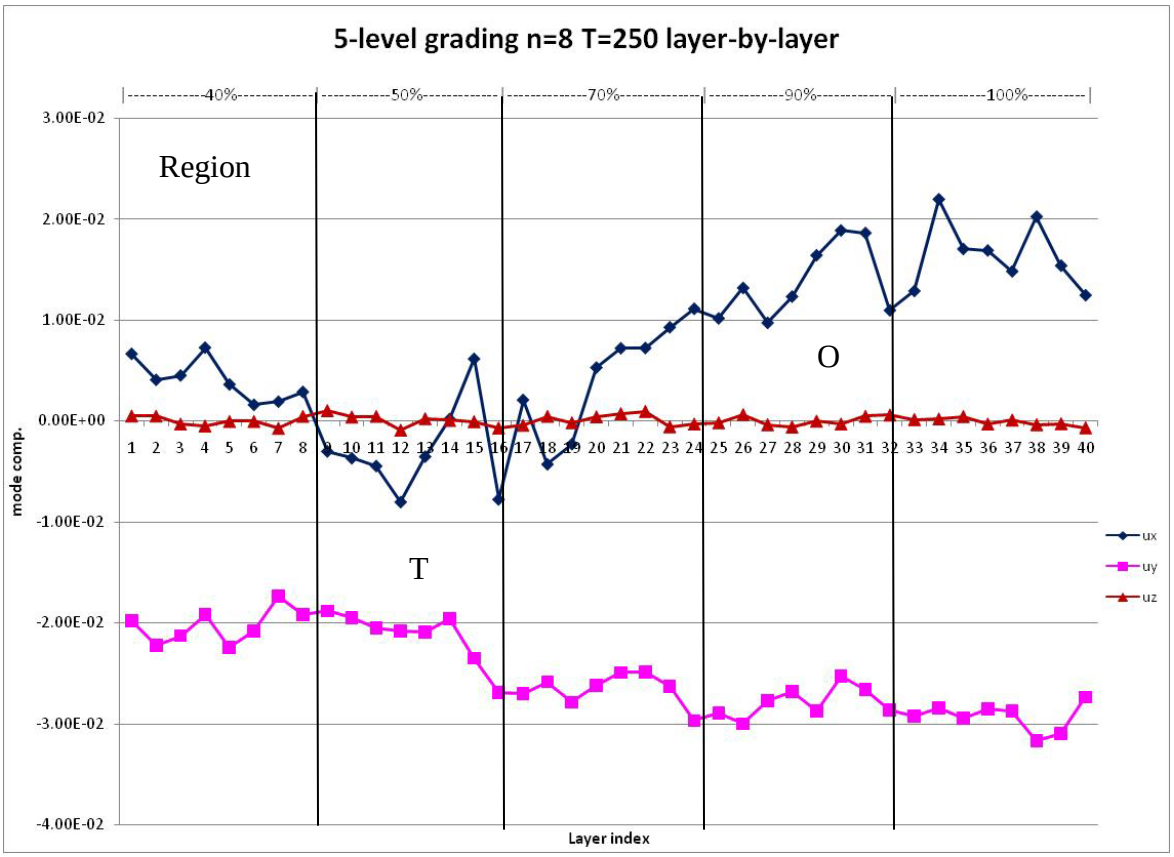

Figure 25: layer-by-layer response of 5-tiered, n=8 at T=250K

Notice that, at the higher temperature (Figure 24), the most Ba-rich layers showed O-symmetry, while the remainder of the material was paraelectric, ($u_x = u_y = u_z = 0$). As temperature decreased, more layers become O-symmetric ($u_x = u_y \neq 0$, $u_z = 0$), but at T=250K, the Sr-rich layers now adopted a T-symmetry ($u_y \neq 0$, $u_x = u_z = 0$) rather than a paraelectric state. This means that, on average, one component of the mode was greater than zero through the whole material, but a second component was greater than zero only through about half of the material. The second component, averaged through the whole

material, was therefore about half the value of the first component, which represented an overall monoclinic phase.

Finally, at temperatures below 200K, (also shown in Figure 26 for 150K) all segments of the system display O-symmetry, completing the transition from paraelectric C-symmetry.

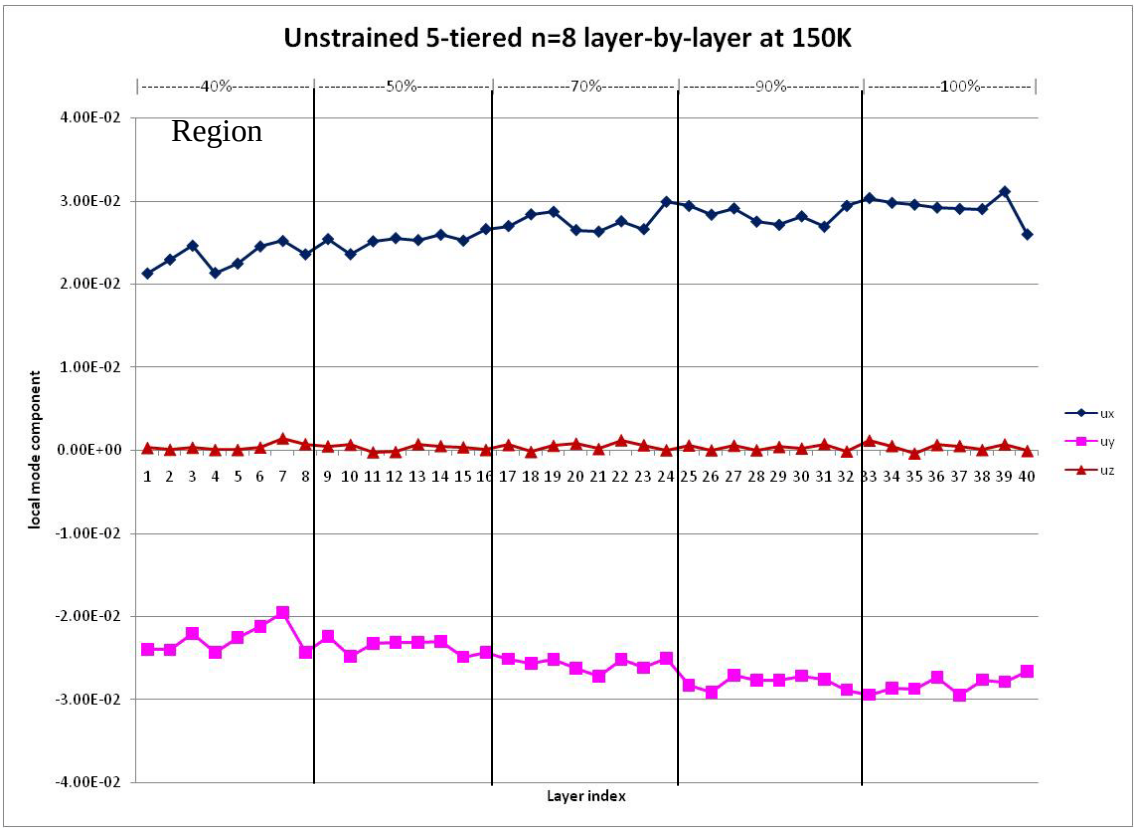

Figure 26: layer-by-layer response of unstrained, five-tiered system with n=8 at 150K.

The overall transition temperature versus region thickness (n) behavior of five-tiered systems is shown in Figure 27:

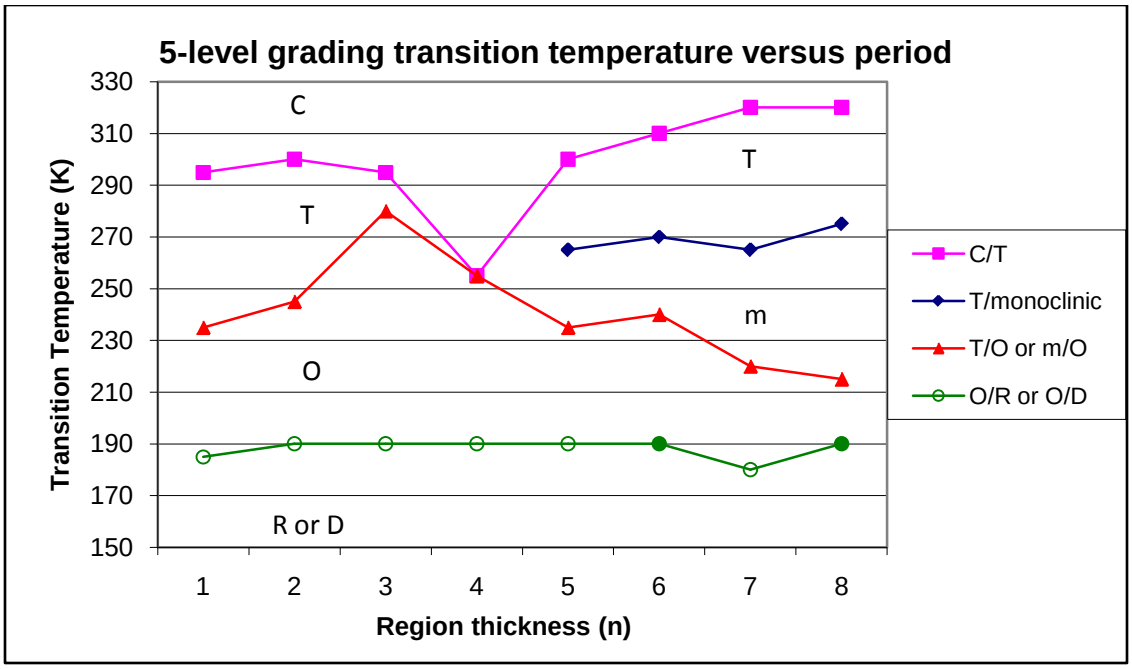

Figure 27: transition temperature versus layer thickness (n) for five-tiered systems. For low-temperature transition, open markers indicate cases where domain stripes were absent, filled markers indicate the appearance of stripes.

Interestingly, there appeared to be a triple-point at n=4, where C, T, and monoclinic phases overlapped. Also, the transition temperature of the monoclinic phase remained essentially constant. At low temperatures, the large-n systems will experience a transition to either an R or D symmetry, depending on whether the system equilibriated to a monodomain (open circles in Figure 27) or striped energy minimum (filled circles in Figure 27).

2. Strained Graded Systems

When the simulated systems were put under epitaxial strain (via the method discussed in Chapter 2, section 2) further changes in behavior relative to bulk and

unstrained systems occured. Simulations were performed which modeled graded BST systems experiencing an epitaxial strain from an $SrTiO_3$ substrate. The results of these simulations are presented below.

A. Two-tiered, Strained Systems

The first significant change in behavior seen when systems were modeled under epitaxial strain is that only one phase transition occured, rather than three. When the system adopted a monodomain, the C-to-T transition appeared, always involving the z-component of the local mode, and further transitions (ie, those involving x- or y-components) were completely suppressed. Such a case is illustrated by the strained n=2 superlattice shown in Figure 28:

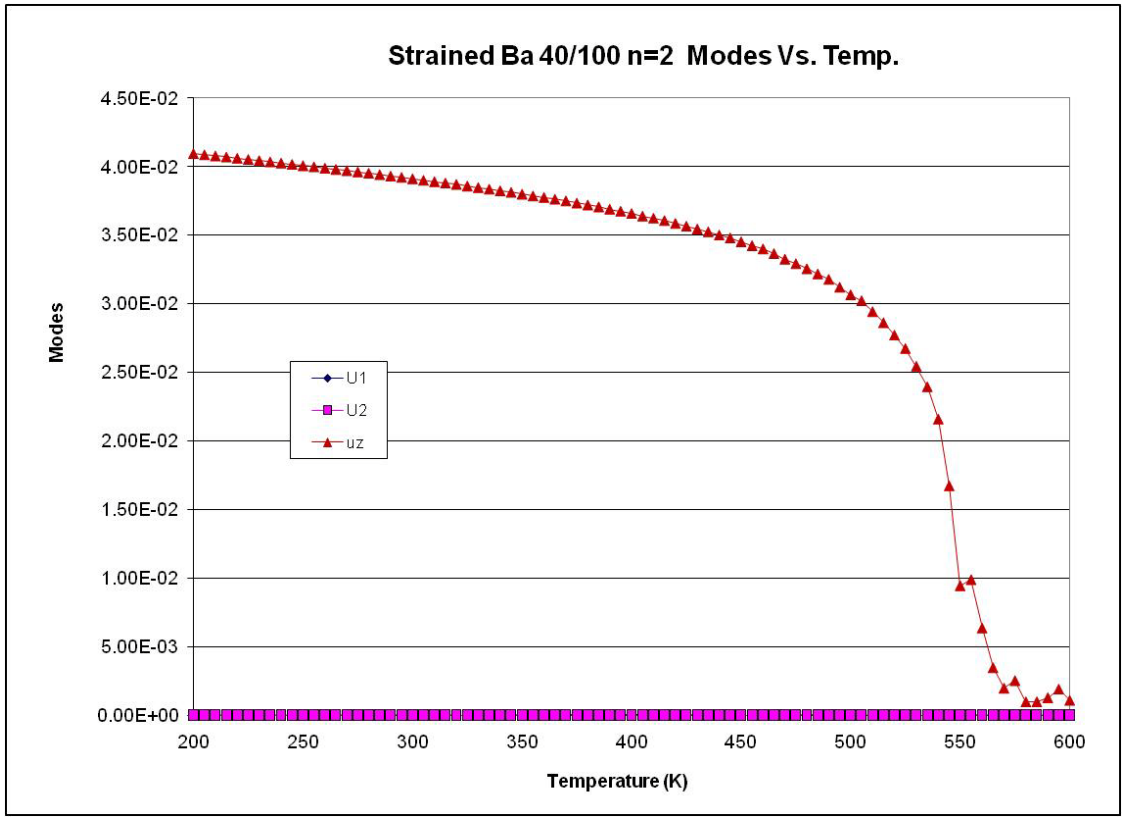

Figure 28: Mode versus temperature behavior of an n=2 strained superlattice.

Such behavior occurred because the system experienced a compressive strain, which heavily favors polarization in the z-direction. Furthermore, for n>3, these systems exhibit vertical striping such as that shown in Figure 29. Notice that, in comparison with Figure 23, striping in the z-component no longer coexisted with any in-plane polarization.

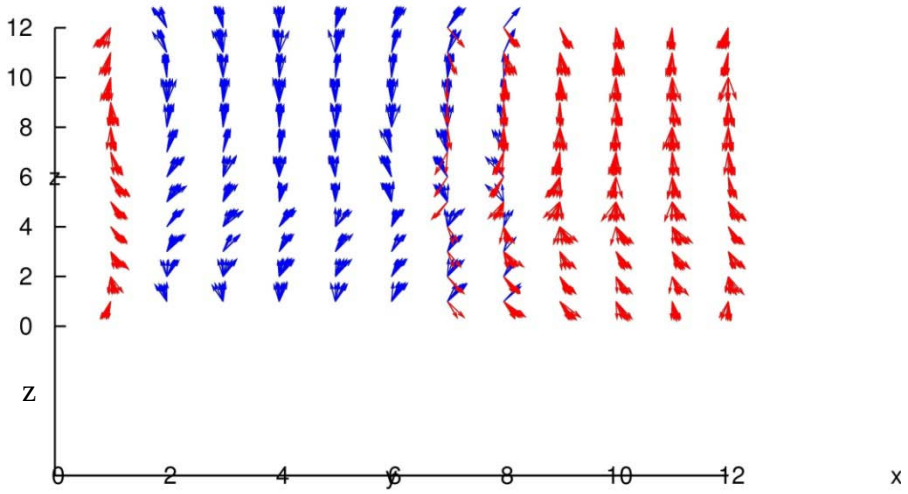

Figure 29: domain striping seen in strained, 40/100 system with n=6

The change in Curie Temperature with respect to region thickness is shown below in Figure 30:

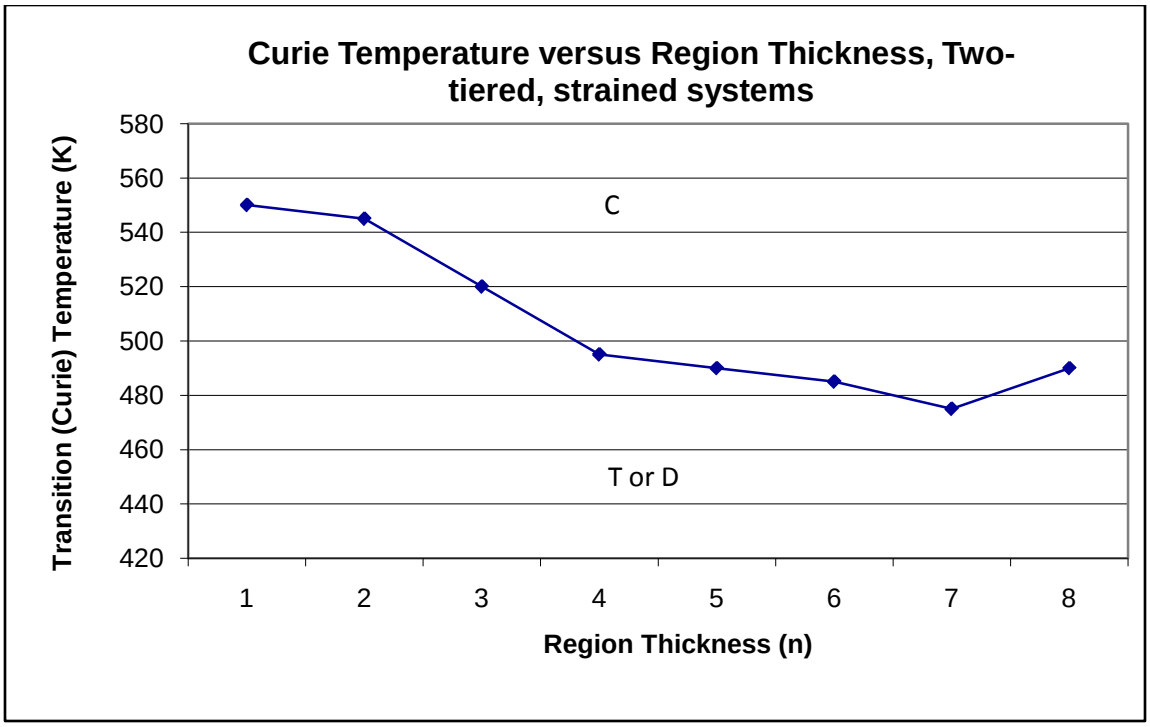

Figure 30: Curie Temperature versus layer thickness in strained systems with two-tiered grading.

As shown, for n=1 and n=2, the Curie Temperature stayed within 5K of 550K. It then decreased, and for n=4 through n=8, the Curie Temperature remains within 15K of 490K. This decrease in Curie Temperature coincided with the appearance of striped domains.

B. Three-Tiered, Strained Systems

For three-tiered grading modeled under epitaxial strain, there is again only a single transition. The behavior of this transition temperature with changing n is illustrated by Figure 31:

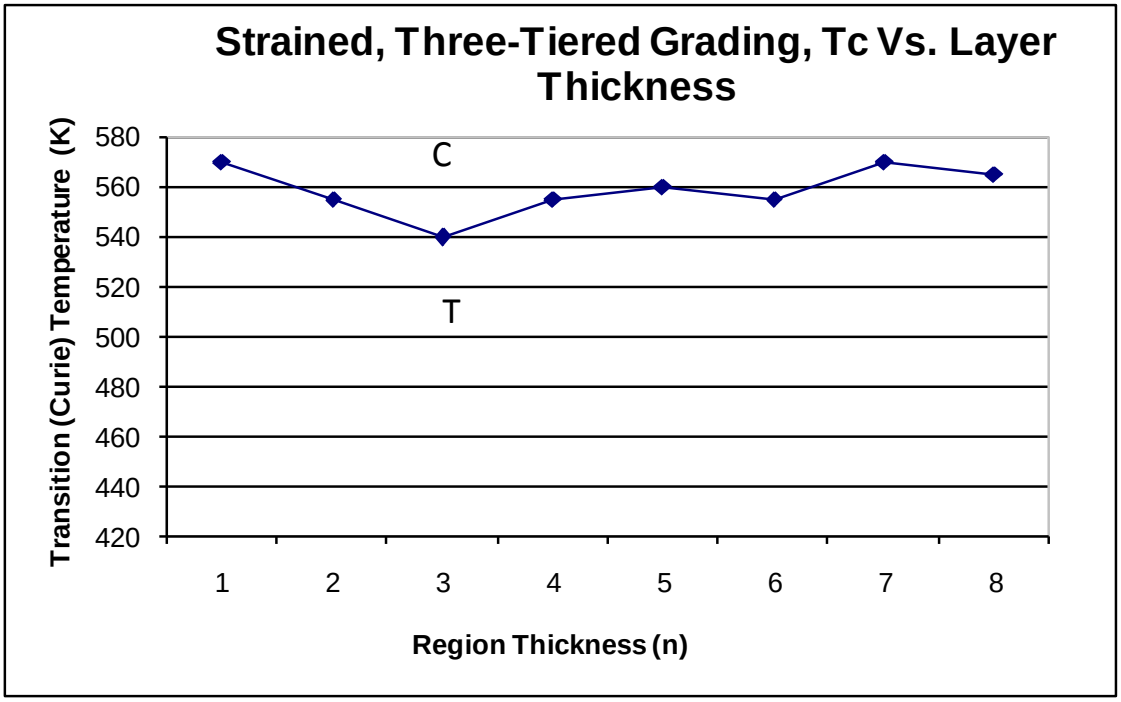

Figure 31: Transition temperature verus layer thickness for three-level grading under strain.

In general, the transition temperature remained in a range between 570K and 555K. Such variation was within the margin of error of ±15K found in the results of the author's Master's Thesis, so it was considered that the transition temperature remains constant with layer thickness for these systems. No striping was evident in these systems.

C. Five-tiered, Strained Systems

For five-tiered systems with n=1 and n=2, only a single transition (C-to-T) was seen. In both cases, the z-component of the local mode increased from zero. However, for larger layer thicknesses, there was domain striping (again involving the z-component of the local mode). These stripes were similar in pattern to Figure 29. It was noted that strained systems not exhibiting stripes have lower energy than equivalent systems exhibiting striped domains, just as in stress-free systems. Also, as in stress-free systems, the local mode self-energy and elastic energy components favored stripes, while the remaining components favored monodomains. The behavior of the Curie temperature versus layer thickness is shown in Figure 32:

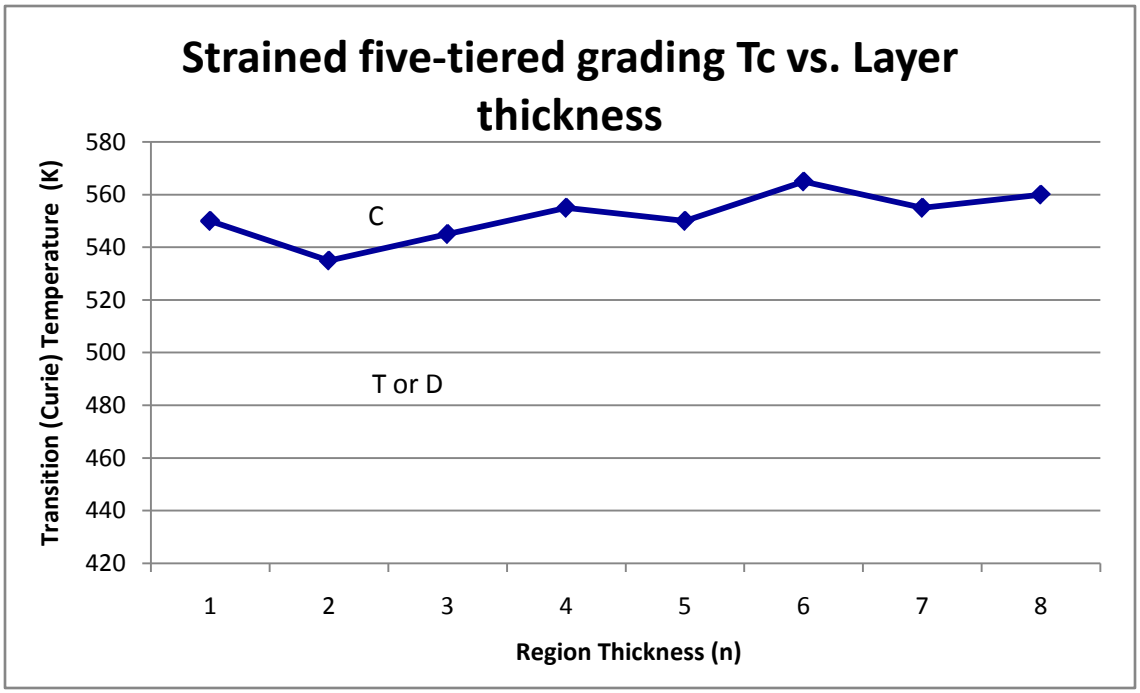

Figure 32: Tc versus layer thickness for strained BST systems with five-tiered grading.

3. Thin-films

Some initial results of stress-free thin-film systems were gathered in order to prove the functionality of the new thin-film code. First, a disordered thin-film of 70% Ba composition which was 12 perovskite cells thick in the z-direction was modeled under ideal OC boundary conditions. The mode-versus-temperature behavior is displayed below in Figure 33:

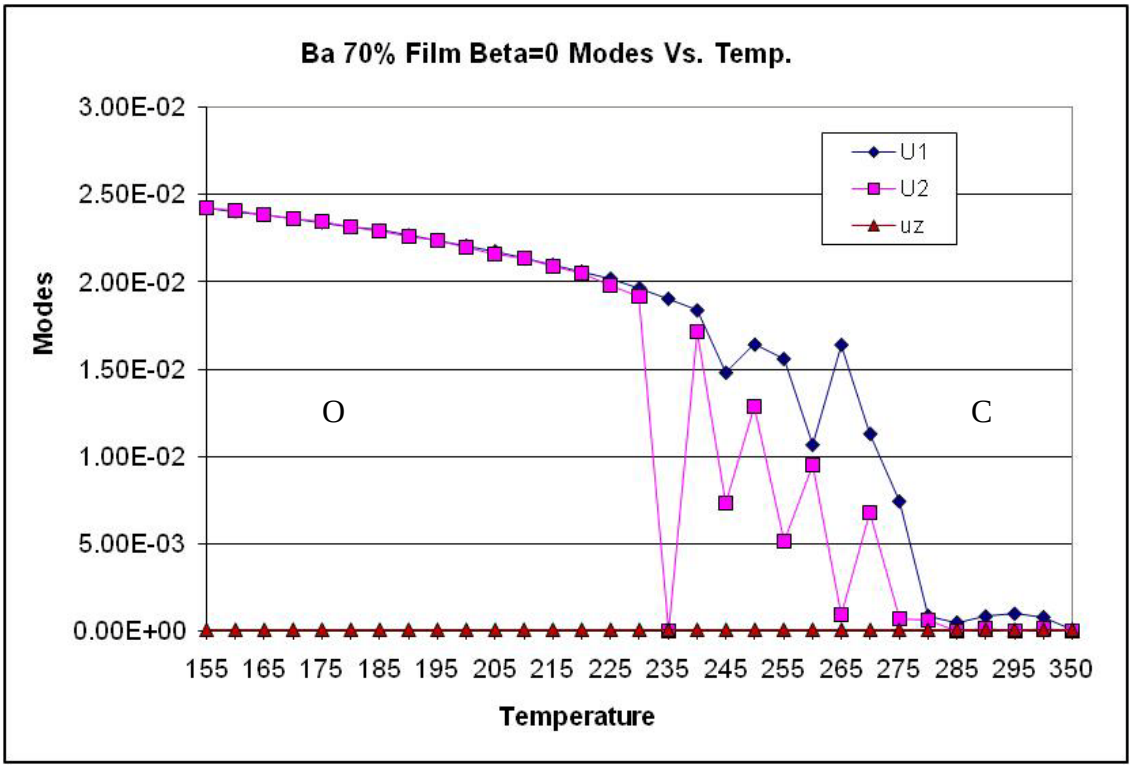

Figure 33: The mode-versus temperature behavior of a stress-free 70% Ba disordered thin-film

It was first noticed that, because of the electrical boundary conditions, the z-component of the local modes always remained zero. A single C-to-O transition was seen around 260K, where both the x- and y-components of the local modes increased from zero. This fell in-between the Cubic-to-Tetragonal and Tetragonal-to-Orthorhombic transition temperatures (305K and 225K, respectively) found in disordered-bulk BST with a composition of 70% Ba. The fact that the system was prevented from reducing its energy by increasing the z-component of the local modes was thought to be responsible for this behavior.

A three-tiered, n=4 graded system was also simulated under ideal OC conditions, and it yielded the results displayed in Figure 34:

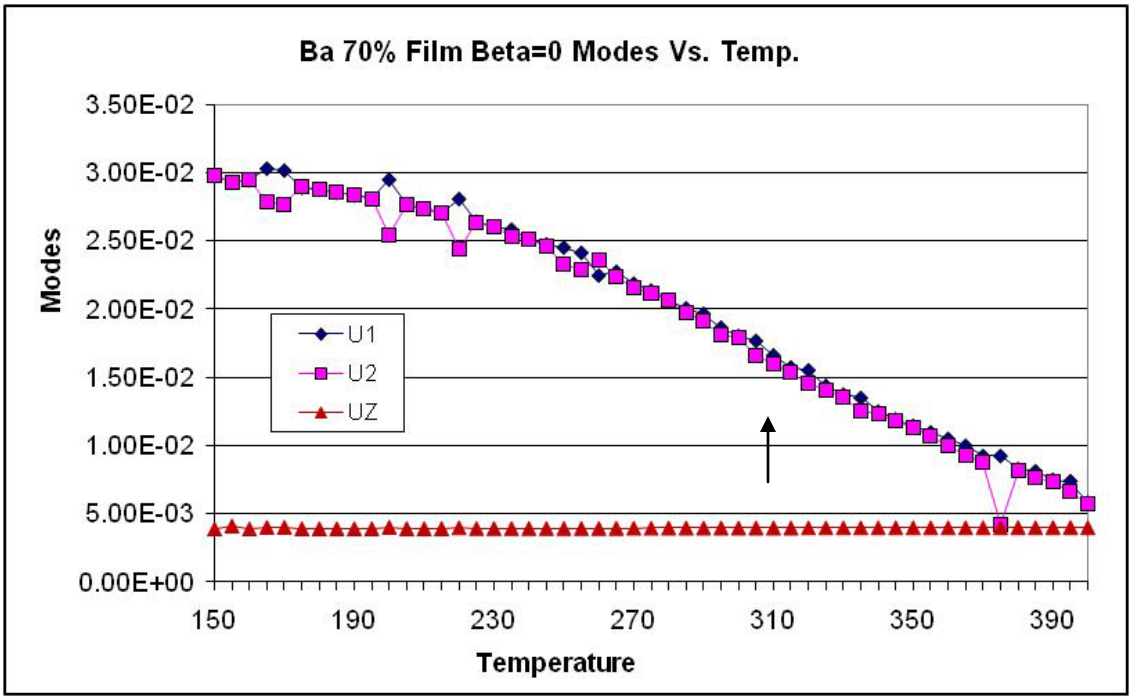

Figure 34: mode-versus-temperature behavior for three-tiered, n=4 graded, stress-free thin-film under OC conditions.

Here, a single C-to-O transition (indicated by the inflection point of the curve, marked with an arrow) was found at 305K . This seemed reasonable, because both the electrical boundary conditions and the grading of the film along the z-axis favored in-plane coordinates of the local mode, making polarization easier and thus raising the Curie temperature. (This observation was supported by recalling the example of Figure 8, where transition temperatures were seen to increase with increasing n). The response of the film was also analyzed layer-by-layer, and this result is shown in Figure 35:

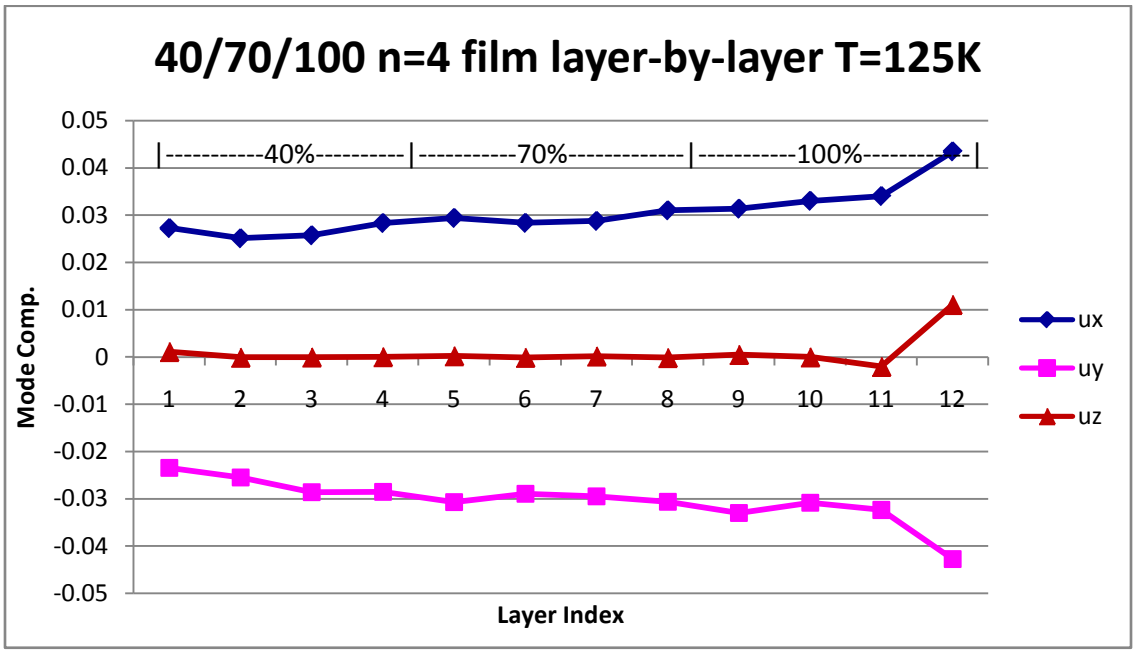

Figure 35: Layer-by-layer response of three-tiered, n=4 film at T=125 K under OC conditions.

Here, it was seen that the magnitude of the x- and y- mode components increased as the Ba concentration increased, which behavior was the same as that of the graded bulk systems (see, for example, Figure 12 or Figure 18). However, one significant difference with respect to bulk graded systems was that, at the top surface, an

enhancement of the polarization was seen, which is consistent with the results found for PZT films in Ponomareva et al. [26] Moreover, the layer-by-layer polarization profile shown in Figure 35 did show an increase in polarization in the more BT-rich layers, but it did not behave like a wave, as in some bulk graded systems (see, e.g. Figure 12), because there was no periodicity along the z-axis in graded films.

Chapter 4: Conclusions and Further Discussion

In qualitative terms, the first general conclusion that is supported by these results was that disordered-bulk systems, graded systems, and systems under epitaxial strain all showed different behavior from one-another. In graded systems, it was shown that the changes in the phase diagram between disordered-bulk and graded systems (such as the merging of T and O transitions and the appearance of a monoclinic phase) generally arose from the fact that, for graded systems with large n, there was a decoupling between regions of different compositions. Changes in behavior also occurred between the different grading schemes (i.e., two-tiered, three-tiered and five-tiered), such as the fact that striped domains began to appear at smaller values of n in the three- and five-tiered systems.

In some cases, domain stripes appeared in graded systems, behavior which was not found to occur in bulk, disordered BST systems. Both the non-striped states (monodomains) and striped states appeared to be stable or metastable. That is, once the system adopted one of the configurations, it would tend to stay in that configuration. Generally, the monodomain cases were found to be of lower energy than the equivalent striped cases.

There were also differences in behavior between stress-free systems and equivalent systems placed under epitaxial strain. Whereas stress-free systems displayed symmetries involving all three components of the local mode, and the z-component consistently increased at the lowest temperature, in strained systems only the z-component was seen to vary from zero. Also, some stress-free systems exhibited horizontal domain striping (except for the five-tiered case, where the stripes had a vertical

orientation), but when striping occurred in systems with epitaxial strain, the striping was always vertically oriented.

All of these results illustrated the power and flexibility of the effective-Hamiltonian modeling method presented in this work. Unstrained, graded sytems were modeled successfully with no alteration to the basic model, and with relatively straightforward modifications, the model was adapted to simulate systems under epitaxial strain and thin-films. This method of modeling also allowed the researcher to examine the layer-by-layer response of the system, which was important for helping to understand why changes in behavior occurred. Such detailed understanding of the systems in question would be hard, if not impossible, to obtain through current experimental methods for characterizing materials.

The basis for modeling thin-films has also been presented here. Thus far, the researcher has seen that the behavior of films did, in fact, vary with respect to the behavior of equivalent bulk systems. A merging of C-to-T and T-to-O transitions was seen, and the Curie temperature was seen to vary from both bulk and between graded and non-graded films. Polarization enhancement at the top surface, and an increasing but non-wavelike layer-by-layer polarization profile was also seen in the graded system presented. Future research may include some refinements to the current model, and a thorough investigation of graded thin-film systems. Also, the same alterations applied to the bulk code to simulate epitaxial strain can be incorporated into the thin-film code, allowing the examination of disordered and graded thin-films under epitaxial strain. Another avenue for future research is the investigation of graded systems with greater

than five-tiered grading, larger n, or systems with an average composition other than 70% BT.

Works Cited

1. **Ahn, K. H., Kim, S. S. and Baik, S.** J. Appl. Phys. Vol. 93 no. 3 p. 1725, (2003).

2. **Menoret, C., et al.** Phys. Rev. B.; vol. 65 p. 224104, (2002).

3. **Mantese, J. V. and Shubring, N. W.** Int. Ferr. vol. 37 p. 245, (2001).

4. **Mantese, J. V. and Alpay, S. P.** *Graded Ferroelectrics, Transcapacitors and Transponents, Multifunctional Thin Fims Material Series.* New York : Springer Verlag, 2005.

5. **Roytburd, A. L. and Slutsker, J.** Appl Phys Lett. vol 89 p 042907, (2006).

6. **Walizer, L., Lisenkov, S. and Bellaiche, L.** Phys. Rev. B.; vol. 73 p. 1144105, (2006).

7. **Walizer, L.** Modeling of Barium Strontium Titanate From First Principles. December 2005.

8. **Zhong, W., Vanderbilt, D. and Rabe, K. M.** Phys. Rev. B.; v. 52 p. 6301, (1995).

9. **Klaus Diagnostics.** *Structure of Perovskites.* [Online] [Cited: April 10, 2009.] http://www.iue.tuwien.ac.at/phd/dragosits/node14.html.

10. **Fu, H. and Bellaiche, L.** Phys. Rev. Lett.; vol. 91 p. 257601, (2003).

11. **He, F., et al.** Phys. Rev. B v. 70 p. 235405, (2004).

12. **Lemanov, V. V., et al.** Phys. Rev. B.; vol. 54 p. 3151, (1996).

13. **Brazier, M., McElfresh, M. and Mansour, S.** Appl. Phys. Lett. vol 72 no. 9 p. 1121, (1998).

14. **Mantese, J. V., et al.** Appl. Phys. Lett. vol. 81 no. 6 p. 1068, (2002).

15. **Tilley, R.** *Understanding Solids.* Chichester, England : John Wilen and Sons, Ltd., 2004.

16. **Kittel, C.** *Introduction to Solid State Physics: seventh edition.* s.l. : John Wiley and Sons, Inc., 1996.

17. Ferroelectric Hysteresis Loop Tracer. *Scientific Equipment & Services.* [Online] [Cited: April 16, 2009.] http://www.sestechno.com/pro1/2a3.htm.

18. [Online] [Cited: November 16, 2005.] http://www.med.unibs.it/~marchesi/pps97/course/section7/os_sol.html.

19. **eSMART SMA/MEMS Research Group.** Smart Materials. [Online] eSMART, August 17, 2001. [Cited: November 21, 2008.] http://www.cs.ualberta.ca/~database/MEMS/sma_mems/smrt.html.

20. *Piezoelectricity of ferroelectric perovskites from first principles.* **Bellaiche, L.** Current Opinion In Solid State and Materials Science, vol. 6 p. 19-25, 2002.

21. **Ban, Z. G., Alpay, S. P. and Mantese, J. V.** Phys. Rev. B vol. 67 p. 184104, (2003).

22. **Felberg, W., et al.** Appl. Phys. Lett. vol. 78 no. 4 p.524, (2001).

23. **Almahmoud, E., et al.** Phys. Rev. B v. 70 p. 220102(R), (2004).

24. **Kornev, I., Fu, H. and Bellaiche, L.** Phys. Rev. Lett. v. 93 p. 196104, (2004).

25. **Bin-Omran, S., Ponomareva, I. and Bellaiche, L.** Phys. Rev. B. vol. 77 p. 144105, (2008).

26. **Ponomareva, I., et al.** Phys. Rev. B vol. 72 p. 140102, (2005).

27. **Naumov, I. I., Bellaiche, L. and Fu, H.** Nature v 432 p. 737, (2004).

28. **Roytburd, A. L., et al.** Phys. Rev. Lett. v 85 p 190, (2000).

29. **Roytburd, A. L. and Slutsker, J.** Appl. Phys. Lett. v 89 p 042907, (2006).

30. **Sepilarsky, M., et al.** Phys. Rev. B v 64 p 060101, (2001).

31. **Zhong, S., Alpay, S. P. and Mantese, J. V.** Appl. Phys. Lett. v 88 p 132904, (2006).

32. **Akcay, G., S. Zhong, B. S. Allimi and Aplay, S.P.** Appl. Phys. Lett. v 91 012904, (2007).

33. **Zhong, S., et al.** Appl. Phys. Lett. 90 092901, (2007).

34. **Nath, R., et al.** Appl. Phys. Lett. v 92 p 012916, (2008).

35. **Zhong, S., et al.** Appl. Phys. Lett. v 89 p 142913, (2006).

36. **Tinte, S., et al.** J. Phys: Cond. Matt v 11 p 9679, (1999).

37. *Theory of the Dielectric Constants of Alkali Halide Crystals.* **Jr, R. G. Dick and Overhauser, A. W.** Physical Review, v 112 no 1 p 90, (1958).

38. **Tinte, S., et al.** Phys. Rev. B.; v. 67 p. 064106, (2003).

39. **Tinte, S., et al.** J. Phys: Cond. Matt v 16 p 3495, (2004).

40. **Akbarzadeh, A. R., et al.** Phys. Rev. B.; vol. 70 p. 054103, (2004).

41. **Ramer, N. J. and Rappe, A. M.** Phys. Rev. B.; vol 62 p. 743, (2000).

42. **Bellaiche, L. and Vanderbilt, D.** Phys. Rev. B.; vol. 61 p. 7877, (2000).

43. **Kornev, L. A. and Bellaiche, L.** Phys. Rev. Lett.; vol. 91 p. 116103, (2003).

44. **Bellaiche, L., Garcia, A. and Vanderbilt, D.** Phys. Rev. Lett.; vol. 84 p. 5427, (2000).

45. **Prosandeev, S., et al.** J. Phys: Cond. Matt. V. 20 p. 193201, (2008).

46. **Lisenkov, S. and Bellaiche, L.** Phys. Rev. B.; vol. 76 p. 020102, (2007).

47. **Tinte, S., et al.** Phys. Rev B v 67 p 064106, (2003).

48. **Neaton, J. B. and Rabe, K. M.** App. Phys. Lett.; vol. 82 no. 10 p. 1586, (2003).

Appendix A: Description of Research Appropriate for Popular Publication

Ms. Walizer and Dr. Bellaiche, scientists at the University of Arkansas, have used a special type of computer simulation called a Monte Carlo program to get a close look at the inner workings of a unique and exciting material known as Barium Strontium Titanate, or BST for short. This material is of interest to scientists because it could potentially be used in many of tomorrow's high-tech devices, including a new form of computer memory.

In order to be able to use BST for high-tech purposes, however, scientists must first be able to understand what it does, how it does it, and why. That's where the simulations come in. Many phenomena in nature, such as the motion of molecules or the absorption of light energy, are what scientists call "statistical processes," by which they mean that they can find equations to describe the "big picture" (e.g., a *whole group* of molecules) but they cannot directly calculate the tiny details of what is happening inside the system, because those tiny details are essentially random. Not only is it impossible to calculate, it is also extremely hard to learn anything about these tiny details by running physical experiments. But, as Ms. Walizer notes, "computers can let scientists see what Nature won't".

A part of the Monte Carlo program called a random number generator can produce a random number between zero and one, and plug that number into the right equations to describe systems that scientists are trying to understand. This lets the

computer mimic the statistical processes found in nature, giving scientists a glimpse of both the big picture and the smaller details of what's going on inside the system.

Walizer and Bellaiche used this kind of simulation to unlock the secrets of BST. BST is actually an alloy, and its properties can be controlled by changing the percentages of the elements Barium and Strontium in the mix. However, scientists are now capable of creating not just an ordinary alloy in the lab, but a so-called graded system, which is a layered alloy whose layers have differing compositions.

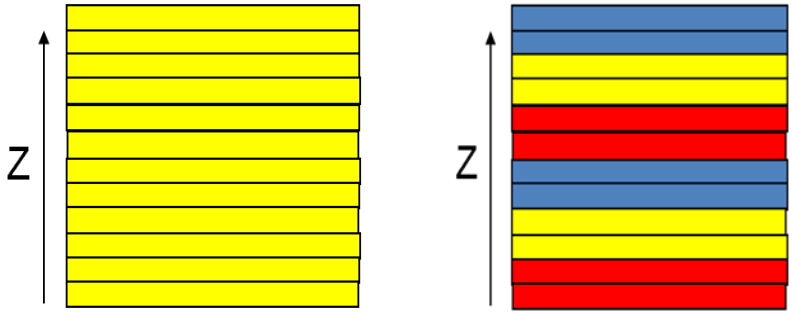

Image 1: comparing an ordinary alloy (left) with a graded alloy (right)

Creating a graded alloy lets scientists customize how the material behaves even better than they can customize the regular alloy by changing its composition. One behavior Walizer and Bellaiche particularly want to examine is the polarization—the separation of positive and negative electric charges—that occurs in graded BST. The simulations they have run showed that when the layers of different composition are thin, the whole material becomes polarized at once, acting like an entirely new alloy, but when the layers are thick, some may become polarized while others do not, with each layer acting independently. This can lead to polarization patterns that aren't seen in non-

layered alloys, and that may make even more technological applications possible, bringing the high-tech gadgets of tomorrow one step closer.

Appendix B: Summary of Newly Created Intellectual Property

1. An existing program for the modeling of the perovskite Barium Strontium Titanate was modified such that it was capable of simulating BST systems under epitaxial strain.

2. An existing program for the modeling of the perovskite Barium Strontium Titanate was modified such that it was capable of modeling two-dimensional BST systems.

3. The data generated by item (1) and the analysis thereof lead to the creation of new knowledge, in the form of knowledge gained about graded and strained BST systems.

4. The data generated by item (2) and the analysis thereof lead to the creation of new knowledge in the form of the initial knowledge gained about BST thin-films.

Appendix C: Patent and Commercialization Opportunities

A. The four items listed in Appendix B are considered from the perspective of whether they are able to be patented.

1. It is possible that this program or its method can be patented or copyrighted, though it should be noted that this method is a modification of a pre-existing code.

2. It is possible that this program or its method can be patented or copyrighted, though it should be noted that this method is a modification of a pre-existing code.

3. The knowledge gained by the use of item (1) involves the properties of BST systems under epitaxial strain. Facts of nature cannot be patented, but novel and useful materials can potentially be patented, so if the properties of some strained BST systems were found to be useful, such systems may be eligible for patenting.

4. The knowledge gained by the use of item (2) involves the properties of two-dimensional BST sytems. Facts of nature cannot be patented, but novel and useful materials can potentially be patented, so if the properties of some low-dimensional BST systems were found to be useful, such systems may be eligible for patenting.

B. The four items in Appendix B are considered from the perspective of their prospects for commercialization.

1. and 2.: As the original code was gained freely without requiring a license, it is unlikely that any form of commercialization would be pursued for the codes comprising items one and two. Commercialization would be distantly possible, but the market would be limited to a small segment of the scientific community.

3. and 4. While devices based on the knowledge comprising items three and four may someday lead to marketable products, the theoretical knowledge itself has very little intrinsic commercial value. It is expected that this knowledge will be shared freely via publication, as is common practice.

C. Prior disclosure of the intellectual property is discussed.

1. and 2. The basis for these methods of modification have been discussed in various published papers, such as those cited in this dissertation. This would likely further decrease the chances of gaining any patents.

3. and 4. The newly gained knowledge arising from the use of (1) and (2) has been presented at the Williamsburg Conference on the Fundamentals of Ferroelectrics, which occurred on February 8-11, 2009. The author and her advisor also intend to publish a journal article based on the work presented in this dissertation, in a publication such as one of the Physical Review series.

Appendix D: Broader Impact of Research

1. Applicability of methods to other problems

The methods used in this research have, in fact, already been applied to studying thin-films of $P(Zr,Ti)O_3$, or PZT, another perovskite alloy. These methods could be easily adapted to other perovskite materials and alloys by adjusting the parameters and the form (where necessary) of the effective Hamiltonian. By using lower-dimensional forms for the dipole-dipole interaction, as discussed in references cited in chapter 2, section 3, the basic method could be further adapted to studying BST nanodots and nanowires, and low-dimensional systems of other perovskite materials and alloys. Further study of the present problem of BST thin-films and graded systems is also made possible by the present research.

2. Impact of research on US and global economy

Because this work was theoretical in nature, no direct economic impact is expected. However, the materials being studied have many possible technological applications (see chapter 1, section 1) and it is hoped that the present study will aid in the eventual realization of these technological applications. As the possible applications are quite broad, the impact of these applications is potentially also broad, but these applications are many years in the future and beyond the scope of the present study.

3. Impact on the Environment

As the research presented in this dissertation is theoretical in nature, no impact on the environment is expected to directly result from any discoveries here presented, unless

one counts the power utilized by the computers running the simulations or the paper utilized printing versions of this dissertation. As actual, practical application of the knowledge presented in this dissertation is expected to be years in the future, and is not within the scope of this dissertation, the economic impacts of device fabrication based on this knowledge are not assessed.

Appendix E: Copy of Microsoft Project Research Project Plan

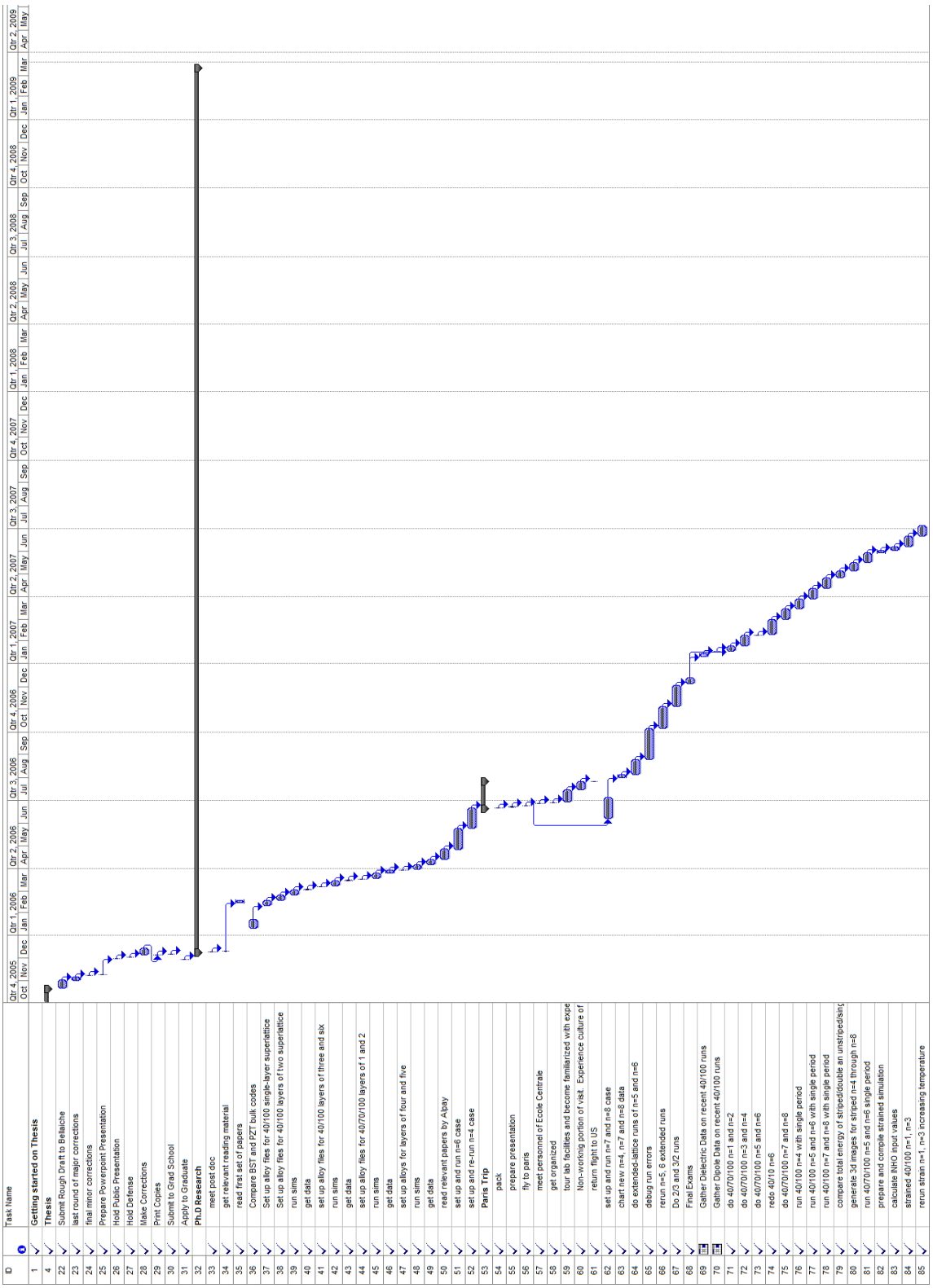

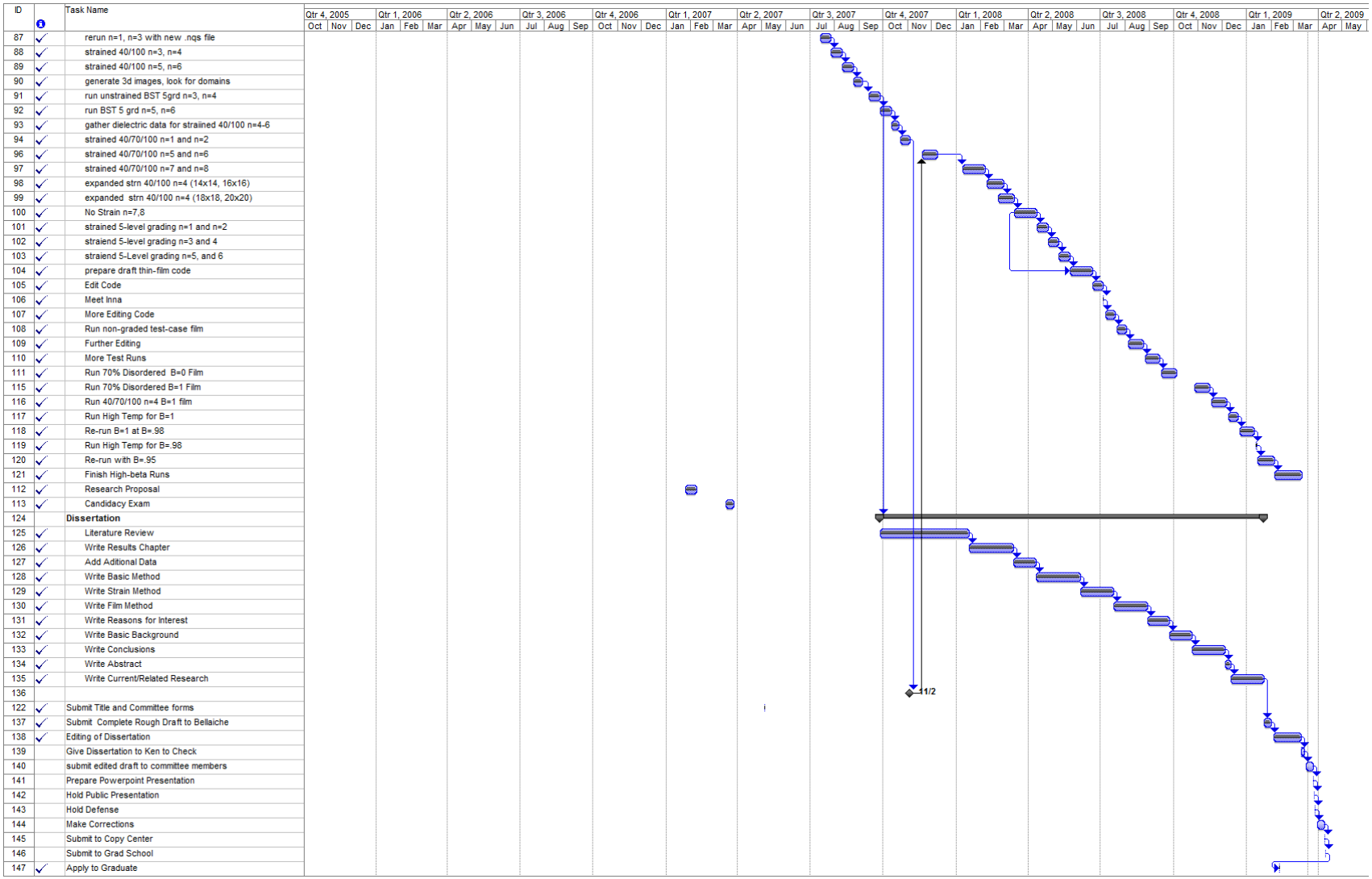

ID		Task Name
87	✓	rerun n=1, n=3 with new .nqs file
88	✓	strained 40/100 n=3, n=4
89	✓	strained 40/100 n=5, n=6
90	✓	generate 3d images, look for domains
91	✓	run unstrained BST 5grd n=3, n=4
92	✓	run BST 5 grd n=5, n=6
93	✓	gather dielectric data for strained 40/100 n=4-6
94	✓	strained 40/70/100 n=1 and n=2
96	✓	strained 40/70/100 n=5 and n=6
97	✓	strained 40/70/100 n=7 and n=8
98	✓	expanded strn 40/100 n=4 (14x14, 16x16)
99	✓	expanded strn 40/100 n=4 (18x18, 20x20)
100	✓	No Strain n=7,8
101	✓	strained 5-level grading n=1 and n=2
102	✓	straiend 5-level grading n=3 and 4
103	✓	straiend 5-Level grading n=5, and 6
104	✓	prepare draft thin-film code
105	✓	Edit Code
106	✓	Meet Inna
107	✓	More Editing Code
108	✓	Run non-graded test-case film
109	✓	Further Editing
110	✓	More Test Runs
111	✓	Run 70% Disordered B=0 Film
115	✓	Run 70% Disordered B=1 Film
116	✓	Run 40/70/100 n=4 B=1 film
117	✓	Run High Temp for B=1
118	✓	Re-run B=1 at B=.98
119	✓	Run High Temp for B=.98
120	✓	Re-run with B=.95
121	✓	Finish High-beta Runs
112	✓	Research Proposal
113	✓	Candidacy Exam
124		**Dissertation**
125	✓	Literature Review
126	✓	Write Results Chapter
127	✓	Add Aditional Data
128	✓	Write Basic Method
129	✓	Write Strain Method
130	✓	Write Film Method
131	✓	Write Reasons for Interest
132	✓	Write Basic Background
133	✓	Write Conclusions
134	✓	Write Abstract
135	✓	Write Current/Related Research
136		
122	✓	Submit Title and Committee forms
137	✓	Submit Complete Rough Draft to Bellaiche
138	✓	Editing of Dissertation
139		Give Dissertation to Ken to Check
140		submit edited draft to committee members
141		Prepare Powerpoint Presentation
142		Hold Public Presentation
143		Hold Defense
144		Make Corrections
145		Submit to Copy Center
146		Submit to Grad School
147	✓	Apply to Graduate

Appendix F: List of Software Utilized in Research

Computer #1:
Model Number: Lenovo Y410
Serial Number: EB06655860
Location: PHYS 237
Owner: Laura Elizabeth Walizer
Software #1:
Name: Microsoft Office 2007
Purchased by: Laura E. Walizer

Software #2:
Name: puTTy
Freeware

Software #3
Name: Internet Explorer 7
Purchased by: Laura E. Walizer

Software #4: Gnuplot
Freeware

Software #5: GSView
Freeware

Computer #2:
Model Number: Dell Dimension 8300
Serial Number: 8654FG32
Location: PHYS134
Owner: Prof. Ken Vickers

Software #1:
Name: Microsoft Office 2007
Purchased by: UA Physics Dept.

Name: Adobe Acrobat Professional 10.0
Purchased by: University of Arkansas Site License

_____ _____

Laura E. Walizer Laurent Bellaiche